$HN_2(^2A')$ Electronic Manifold. II. *Ab Initio* Based Double-Sheeted DMBE Potential Energy Surface via a Global Diabatization Angle

Vinícius C. Mota and António J. C. Varandas*

Departamento de Química, Universidade de Coimbra, 3004-535 Coimbra, Portugal

Received: November 5, 2007; In Final Form: January 18, 2008

A double-sheeted double many-body expansion potential energy surface is reported for the coupled $1^2A'/2^2A'$ states of HN_2 by fitting about 6000 *ab initio* energies. All crossing seams are described to their full extent on the basis of converged results. The lowest adiabatic sheet is fitted with a rmsd of 0.8 kcal mol^{-1} with respect to the calculated energies up to 100 kcal mol^{-1} above the absolute minimum, and the topology of the first excited-state investigated with the aid of the upper adiabatic sheet. A new scheme that overcomes obstacles in previous diabatization methods for modeling global double-sheeted potential energy surfaces is also reported. The novel approach uses a global diabatization angle which allows the diabats to mimic both the crossing seams and atom−diatom dissociation limits.

1. Introduction

The ground state of the title system has been the target of several theoretical studies[1−3] in recent years, mostly aiming to establish reliable estimates for its lifetime as it has been postulated[4] as a product of the reaction

$$NH_2 + NO \rightarrow \text{products} \qquad (1)$$

a primary step on the thermal De−NO_x process. Although previous estimates of such a lifetime[1,3] consistently fall into the range 10^{-9}−10^{-11} s, significant discrepancies persist between the theoretical and experimental estimates,[3] with an important source of error being likely due to the neglect of nonadiabatic effects.[1,3] This conjecture is supported by the disagreement observed in trajectory calculations[3] for the $N + NH \rightarrow N_2 + H$ reaction, despite the fact that the reported single-sheeted potential energy surface[2,3] (PES) reveals a high-degree of accuracy. The unavailability of a multisheeted PES[5] then forbids any evaluation of such nonadiabatic effects. Our main goal in this paper is therefore to model a global double-sheeted PES, a natural step to follow our recent *ab initio* study of the title system in ref 5.

To construct a multisheeted PES,[6−8] we have proposed two approaches[9−11] that utilize in one form or another a double many-body expansion (DMBE)[7,8,12−14] theory; for references to single-sheeted forms including larger polyatomic systems, the reader is referred to ref 15. In this theory, we have suggested for the first time to split the potential energy into its various short- and long-range components followed by a development of each term as a cluster or MBE[6] expansion. The DMBE strategy conforms therefore with the traditional perturbation theory partition of the interaction energy into short- and long-range contributions or else with the molecular-orbital (MO) theory view of partitioning the total energy into an extended-Hartree−Fock contribution that includes the nondynamical correlation and the dynamical correlation itself. Thus, every term in the DMBE can be expressed such as to conform with its correct asymptotic dependence on the interatomic distance(s). The first of the above-mentioned multisheeted formalisms utilizes the diatomics-in-molecules (DIM)[16−18] theory to construct the base potential matrix and introduces many-body terms via dressing of the diatomic states.[7,19,20] As a result, this approach is also known as the dressed-DIM[7] method. The second approach uses the standard strategy pioneered by Murrell and co-workers[6] for directly modeling the diabatic potential matrix but uses DMBE (rather than MBE) to model the various matrix elements. For H_3^+, the dressed-DIM formalism has led to a highly accurate PES[11] that improved significantly over previous DIM-related forms for the three lowest states of this molecular ion.[21,22] The same technique has been applied to NO_2, yielding an accurate description of the first two doublet A′ states.[10] Unfortunately, despite its appealing quantum background, the use of a minimal basis set leads for NO_2 to a 8×8 potential matrix, which requires handling 64 matrix elements and hence complicates its application in dynamics (recall that the diagonalization time scales with the cube of the matrix dimension).

For HN_2, no dressed-DIM construct has been reported. Since our purpose here is a description of the intricate topology of the first two A′ states as described in detail elsewhere,[5] we have chosen to follow the strategy of modeling a 2×2 diabatic matrix within standard DMBE theory. The accuracy of such an approach depends, however, not only on the formalism employed but also on how the adiabatic *ab initio* calculations are assigned to the diabatic matrix elements. Thus, a careful analysis of the advantages and drawbacks of previous diabatization schemes[23−38] as applied for the construction of global multisheeted PESs with polynomial techniques is justified due to being unavailable thus far. This will be given in section 2, with the rest of the manuscript being organized as follows. Section 3 describes how the multireference configuration interaction[39] (MRCI) points[5] employing the aug-cc-pV*T*Z (AV*T*Z) basis set of Dunning[40,41] are corrected by the DMBE-SEC[42] method to account for excitations beyond singles and doubles and for basis set incompleteness, while the diabatization scheme is discussed in section 4. Details on DMBE[7,12−14] modeling of the diabats are given in section 5, and the results discussed in section 6. Section 7 gathers the conclusions.

* Corresponding author. E-mail address: varandas@qtvs1.qui.uc.pt.

10.1021/jp710610d CCC: $40.75
Published on Web 04/02/2008

2. Global Multisheeted Approaches Employing Diabatization Schemes: A Synopsis

A wide variety of methods for producing diabatic states[43−46] has been reported in the literature,[23−38] followed by many multisheeted PESs.[9,29−35,47−55] For convenience, we divide them in two categories. The first gathers approaches that yield directly the diabatic states,[23−35,36] either from *ab initio* energies or diabatic electronic wave functions, thus without an intermediate step. The second class includes methods that obtain the diabatic states from the analysis of the behavior of separate molecular properties[36−38] such as dipole or transition moments.

The direct diabatization methods which are based[23−26] on finding electronic wave functions (and subsequently molecular properties[57]) that behave smoothly at the neighborhood of conical intersections, where the adiabats are known to vary drastically and often in a discontinuous manner, frequently yield diabatic states without a well-defined behavior at the atom−diatom asymptotes. From a first-principles investigation of the photodissociation on the Chappuis band of ozone, Woywod *et al.*[47] applied a method[23,24] for obtaining smoothly varying complete-active-space self-consistent-field (CASSCF) wave functions by employing MO theory with nearly constant linear combination of atomic orbital (LCAO) coefficients, followed by block-diagonalization[27] of the Hamiltonian, to obtain slowly varying configuration interaction (CI) coefficients. By interpolating the resulting diabatic points,[47] they were able to achieve highly non-varying diagonal diabatic representations for the $1^1A''/2^1A''$ states of O_3, which have been subsequently employed in dynamics calculations.[58,59] Among the prominent features of the reported states[47] [covering wide regions of configuration space, also for the $1^1A'$ ground state and transition dipole moment (TDM) surfaces], we note that the diabats fail to merge the adiabats at the atom−diatom limits (the off-diagonal diabatic term is nonvanishing at those limits since the adiabatic states can be recovered at any geometry through a diabatic-to-adiabatic transformation). Quoting the authors,[47] "...we have to decide where in nuclear coordinate space we want the diabatic representation to coincide with the adiabatic representation.... it appears natural to require that the diabatic states merge asymptotically with the adiabatic states of the fragments... this definition would not lead, however, to a diabatic representation which eliminates the singular part of the NAC at the conical intersection. We have therefore adopted the alternative option of requiring the diabatic basis to coincide with the adiabatic basis on the C_{2v} symmetry line... These adiabatic states, consequently, do not merge with $O + O_2$ adiabatic states asymptotically...". In a more recent application to the $1^1A''/2^1A''$ states of O_3, Nakamura and Truhlar[26] reported a generalization of the diabatization method proposed by Atchity and Ruedenberg.[25] They have observed a similar behavior for the diabats at dissociation, although for LiFH[26,60] such states do appear to behave as expected at the asymptotes.

In an early attempt to establish a purely first-principles understanding of the photodissociation of H_2S, Heumann *et al.*[48] suggested a procedure for constructing mixing angles by exploring at each geometry the CI coefficients of the reference configurations that have the desired diabatic character at the locus of C_{2v} symmetry. Their *ab initio* calculations[61] covered a broad area of configuration space for the coupled $1^1A''/2^1A''$ states, ground state ($1^1A'$) as well as TDM surfaces, followed by construction of a sequence of interpolated PESs for the three diabats, adiabats, and TDM surfaces. In fact, their calculations allowed a satisfactory description of the first absorption band of H_2S. However, as noted in ref 48, the resulting mixing angles do not show a correct asymptotic behavior, with the diabats not merging the adiabats at the atom−diatom dissociation limits. Using a similar diabatization scheme, Dobbyn and Knowles[38] have reported the same difficulty in a study of the $^1A'$ states of the water molecule. In turn, Simah *et al.*[49] reported a new first-principles study of to the coupled $1^1A''/2^1A''$ states of H_2S, where they attempt to correct for failures of the previous study for the same system.[48] By aiming at a substantial improvement on the quality of the *ab initio* description of the crossing seams and avoided crossings of higher excited states, they have employed a larger basis set with polarized functions and more excited states (one $^1A'$ state and seven $^1A''$ states on the CASSCF calculations, followed by one $^1A'$ state and three $^1A''$ states in the subsequent MRCI calculations). A large number of geometries has been computed with the new diabatization scheme. On the basis of the principle of near spatial invariance of the CI diabatic coefficients, they have generalized the method of Domcke et al.[23,24] by maximizing also the overlap $|\langle\phi_i(q')|\phi_i(q)\rangle|^2 + |\langle\phi_j(q')|\phi_j(q)\rangle|^2$ for all i, j MO pairs at the current (q) and neighbor (q') geometries. Although the qualitative picture remains identical to the previous one,[48] a high quantitative improvement has been observed in the subsequent dynamics study. However, a large discrepancy between the adiabats and diabats remains at the dissociation limits, which has been interpreted as "an artifact of the diabatization procedure", and referred as an "unavoidable effect".

Also for H_2S, Köppel *et al.*[62] have implemented the diabatization procedure of Thiel and Köppel,[28] where the main idea is to remove only the part responsible for the singularities from the nonadiabatic coupling term via a unitary transformation. Their results were compared with those of Simah *et al.*,[49] showing that their diabats do not merge either the adiabats at the HS−S dissociation channel. In turn, Mahapatra *et al.*[63] reported a PES for the lowest two $^2A'$ states of NO_2 by employing the same scheme, with 315 *ab initio* points reported for regions relevant to photodissociation in addition to further calculations to map the conical intersection. Although satisfactory in this region (the points have been interpolated), it is not clear whether their surfaces describe the atom−diatom dissociation limits.

A key feature of modeling strategies that employ MBE[6,8] is that the electronic states, either adiabatic or diabatic, must have a well-defined behavior at the asymptotes. As a result, the topology of the diabats obtained from the above direct diabatization schemes[23−28,48,49] at the asymptotes represent a serious drawback for MBE[6,8] modeling. We remark that the authors have themselves revealed skepticism on the hypothesis of obtaining diabats that simultaneously account for the crossing seams, show a vanishing diabatic coupling element $< \phi^d|\nabla_{\mathbf{R}}|\phi^d >$ (producing smoothly varying electronic wave functions over the whole configuration space), and merge the adiabats at the asymptotes. Because this last issue is critical for dynamics, the diabatic angle obtained from the above schemes[23−28,48,49] has often been artificially corrected such that the diabats so obtained show the proper asymptotic limits. In particular, when using the O_3 PESs of Woywod *et al.*,[47] Flöthman *et al.*[58] fitted the mixing angle to analytical expressions while polynomial forms were utilized for the adiabats at the atom−diatom limits. The diabatic description of this region, obtained by cubic-spline fitting a grid of points originating from the fits of the mixing angle has then been merged via switching forms with the diabats earlier obtained. Other modifications proved necessary. For H_2S,[48] the mixing angle τ has been empirically written as $\tau = \tau_{\text{calc}}[1 - f(\mathbf{R})] + \pi/2 f(\mathbf{R})$, where τ_{calc} is the actually calculated

(asymptotically non-vanishing) mixing angle, and $f(\mathbf{R})$ a switching function that enforces the diabats to merge the adiabats at the H + HS asymptote. Analytical forms to fit the mixing angle have been used by Kurkal *et al.*[50] for the double-sheeted PES of $NO_2(^2A')$ with the diabatization scheme of Simah *et al.*[49] However, variations with the α valence angle of up to 5.7 kcal mol^{-1} near the atom−diatom asymptote are observed for both diabats and adiabats. Grebenshchikov *et al.*[51] followed a similar strategy to study the Chappuis band of ozone, with the diabatic angle being obtained with the scheme of Simah *et al.*[49] and fitted as for NO_2.[50] Here too, the diabats do not merge the adiabats at the atom−diatom limits.

Another direct diabatization scheme pioneered by Murrell and co-workers[6,29−31] imposes the correct atom−diatom behavior of both diabats and adiabats by writing as MBE, DMBE or modified London-Erying-Polani-Sato (LEPS)[64−66] forms the diagonal elements of a standard 2 × 2 diabatic matrix,

$$\begin{pmatrix} V_{11} & V_{12} \\ V_{12} & V_{22} \end{pmatrix} \tag{2}$$

The off-diagonal term is chosen to warrant that the eigenvalues of the above matrix

$$V^{\pm} = \frac{1}{2}(V_{11} + V_{22}) \pm \frac{1}{2}\sqrt{(V_{11} - V_{22})^2 + 4V_{12}^2} \tag{3}$$

reproduce the adiabats to the desired extent. For H_2O, after expanding the diabats with the MBE formalism, Murrell and co-workers[30] obtained a zeroth-order representation of those terms by considering regions where the off-diagonal term is known to be zero or very small and the diabats can be assumed to coincide with the adiabats, e.g., at linear arrangements and points approaching the atom−diatom dissociation limits. The off-diagonal term is written as the product of a three-body polynomial in the interatomic coordinates by damping functions that kill the latter both at the atom−diatom limits and at linear geometries. Equation (3) will then yield adiabats that reproduce the conical intersection seam while dissociating correctly at the various atom−diatom limits. Regions where V_{12} should be important (*e.g.*, those with C_s symmetry) have been used for obtaining the data necessary to model the off-diagonal term. All zeroth-order solutions have finally been used in a nonlinear least-squares fit to their relatively small (in modern standards) number of adiabatic *ab initio* energies via eq 3. The resulting adiabats fit the known topological features including the conical seam, with the diabats properly merging the adiabats at the atom−diatom limits. A refit of the H_2O PESs to a larger number of *ab initio* points with the DMBE method has been reported,[52] although it is unclear whether a significant improvement has been achieved in comparison with the previous[30] PES.

A similar approach has been employed in a series of double-sheeted PESs[32−34] for the interaction of metal atoms with covalent diatomics. In all cases, a diabatic matrix as in eq 2 has been used, with the diagonal states modeled by LEPS forms. For NaFH, Topaler *et al.*[32] utilized a functional form for the off-diagonal term that could account for the correct diatomic coupling at the atom−diatom limits as determined by using transition dipole moments.[37] The authors were the first to note that a reasonable approach for obtaining points that represent such a state would be by setting the seam of avoiding intersections of the adiabats (the line of minimal gap) as if they were lines of diabatic crossings. According to eq 3, this would give $V_{12} = (V^+ - V^-)/2$ at such geometries. The off-diagonal terms were then fitted to the points so generated using a non-

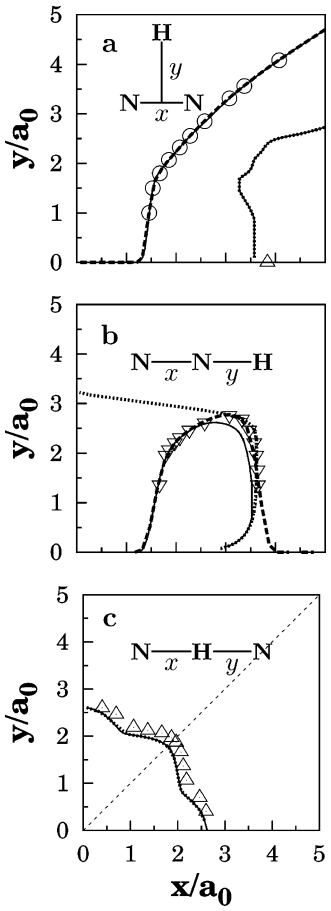

Figure 1. Key for predicted crossing seams: (—) $\alpha(\mathbf{R})$; (— —) α_{H-N_2}; (---) α_{N-NH}. Key for *ab initio* crossing seams: (○) T-shaped; (▽) NNH; (△) NHN.

vanishing form, which prevented a more satisfactory description of the conical intersections. Note that the position for minimum energy gap shown in their paper does not always correspond to the location of the avoided intersections (this is clear from Figure 2 of ref 32, which shows that the minimum energy gap does not coincide with the adiabatic crossing seam for linear arrangements). A final remark to observe that no electronic structure calculations have been performed for the NaH + F channel (mostly because it is energetically inaccessible), and that the diatomic coupling was allowed to vary along the fit for this channel. Similar steps have been followed by Hack and Truhlar[33] to construct a double-sheeted PES for NaH_2. They modeled the diabats using modified LEPS forms, and added long range forces to them. The off-diagonal term has been designed and fitted as in ref 32, and held constant along the rest of the fit. A notable difference from ref 32 refers to the off-diagonal term that has been chosen to vanish at any geometry with C_{2v} symmetry, where the locus of conical intersections lies. Using such an approach, they have been able to model the crossing seam over part of the C_{2v} domain. However, despite the use of a large number of *ab initio* points, the authors acknowledge[33] the method's inability to attain quantitative accuracy over the whole configuration space, which led them to focus on the exciplex and neighborhood of the crossing seam which have been judged as the most relevant regions for their purpose. More recently, Jasper *et al.*[34] reported a PES for LiFH following a similar approach. Modified LEPS forms with long range forces have been used to model the diabats, while the functional form of the strictly nonvanishing off-diagonal term[32] has once more been obtained from the requirement that the

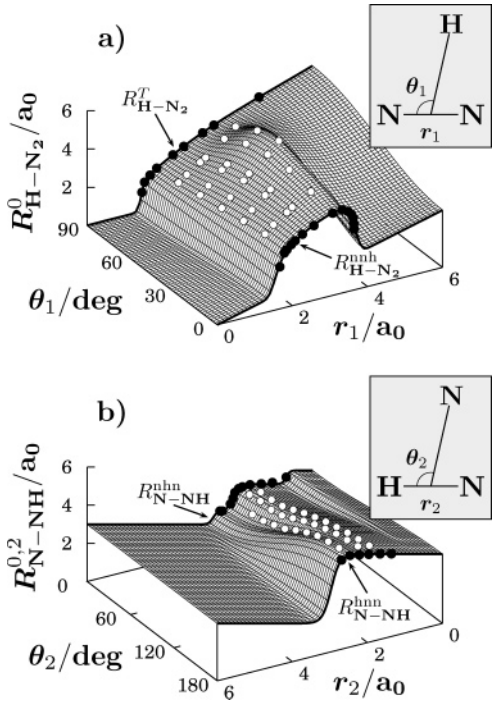

Figure 2. Adiabatic avoided intersections in Jacobi coordinates. (**a**) channel H−N_2; (**b**) channel N−NH. Solid circles represent *ab initio* calculations for the crossing seams from ref 5, and white circles represent avoided intersection estimates from the adiabatic *ab initio* points (see text).

correct diatomic coupling were mimicked at the dissociation limits. This term was fitted to points generated as before[32,33] and considered as a zeroth-order solution. The parameters in it, and in the diagonal diabatic states, have then been allowed to simultaneous optimization in a final nonlinear fit using a large number of *ab initio* points.

A handicap of the above approaches[6,29−34] is that the calibration of the diabats is not done by fitting diabatic energies. The diabats are rather obtained via an indirect fit of eq 3 to adiabatic energies. This requires ingenious albeit restrictive methods for guessing the zeroth-order solutions of such diabats. In the application to H_2O by Murrell *et al*.,[30] only certain regions of the configuration space have indeed been used for such a purpose, mostly because the authors wished to illustrate the method. Similar applications[32,34] but the one for NaH_2[33] do not yield strictly global PESs (*i.e.*, quantitatively describing all channels).

The final type of direct diabatization here considered is a procedure introduced by Hay *et al*.[35] for the study of the photodissociation of ozone in the Hartley band.[35,53,54] These authors have labeled the electronic states according to its classification at C_{2v} arrangements (where the diabatic states can be exactly identified), and reassigned the adiabatic energies into diabatic ones. Each adiabatic energy was then identified "by eye" as belonging to one of the diabatic states in the neighborhood of arrangements with C_{2v} symmetry. The same has been done for arrangements far from the strong coupling region (e.g., atom−diatom limits), and the resulting diabatic states fitted with the MBE[6] method. Despite the satisfactory results,[54] the procedure is somewhat simplistic[67] in the sense that there is no rigorous way of recovering the adiabatic states. It can though be justified due to the complexity arising from at least four electronic states with $^1A'$ symmetry strongly coupled by several seams of conical intersections. As noted,[54] a rigorous electronic structure study including a full modeling of the adiabatic or diabatic topological features would be an "Herculian task".

Indirect diabatization schemes[36−38] offer the interesting possibility of providing at low cost[38] the diabatization angle from the analysis of a molecular property other than the energy. The diabats so obtained would imply almost no additional cost but the calculation of the adiabats, and would be reliable wherever such diabatization angle were valid. The conditions to be satisfied for usefulness of a given property as a diabatization criterion were formally discussed by Macias and Riera,[36] and a review on methods for diabatizations of this type can be found elsewhere.[38] From their work, Dobbyn and Knowles[38] have concluded that the use of a transition angular momentum employing a third state uncoupled from the others appears as the most promising route. However, even for this property, artificial corrections on the diabatization angle may be required, although minor. That might represent a drawback for such schemes. Dobbyn *et al*.[55] reported a PES for the first two $^1A'$ and lowest $^1A''$ states of HCl_2, where the adiabatic points were diabatized via transition angular momentum and then fitted them to a rotated-Morse cubic-spline form. It is difficult to fully assess the merits of their diabatization procedure, since the grid of points covered mostly the valence region. Indeed, the rotated-Morse cubic-spline forms used for the diabats where subsequently merged[68] with asymptotically correct forms to provide a reliable representation. Another PES employing a diabatization method based on molecular properties (the dipole moment) has been reported by Boggio-Pascua *et al*.[9] for the first two $^2A'$ states of C_2H. As in ref 38, modifications had to be done on the diabatization angle to correct the asymptotic behavior and spurious diabatic crossings away from linearity where the locus of conical intersection lies. The diabats were then modeled using DMBE theory. Despite the good accuracy of the fit, the extent of agreement between the predicted and calculated crossing seams has not been discussed in detail preventing further appreciation.

3. *Ab Initio* Energies Revisited

The major topological features of the coupled adiabatic states $1^2A'$ and $2^2A'$, including the seams of conical intersection, have been covered by the grid of 3000 *ab initio* geometries reported in ref 5, which extend over the regions defined by $1.5 \leq r_{N_2}/a_0 \leq 4.0$, $1.0 \leq R_{H-N_2}/a_0 \leq 10.0$ and $0 \leq \gamma/\text{deg} \leq 90$ for H−N_2 interactions, and $1.3 \leq r_{NH}/a_0 \leq 3.3$, $1.0 \leq R_{N-NH}/a_0 \leq 6.0$ and $0 \leq \gamma/\text{deg} \leq 180$ for N−NH interactions; r, R, and γ are atom−diatom Jacobi coordinates. The calculations have been carried out at the MRCI level of theory including single and double electronic excitations using state averaged full-valence-complete-active space (FVCAS)[69] wave functions as the reference, and employing the AV*T*Z basis set. Such calculations recover only a portion of the electronic dynamical correlation, and hence energy barriers and other stationary points, as well as relevant thermodynamic quantities, may suffer from significant errors.[70] Furthermore, the amount of dynamical correlation recovered by the MRCI calculations may differ with the electronic state, changing the relative positioning of the various states and hence the loci of the crossing seams, as observed in the case of ozone.[47] Since part of the dynamical correlation will unavoidably be missing in any MRCI calculation (but in the case of a full CI expansion), one is led to believe that also the loci of crossing seams are subject to improvement.

In this work, we have used the DMBE-SEC[42] method to correct the calculated MRCI energies for the incompleteness of the basis set and truncation of the CI expansion. For each adiabatic state, the DMBE-SEC energy assumes the form

$$V(\mathbf{R}) = V_{\mathrm{FVCAS}}(\mathbf{R}) + V_{\mathrm{SEC}}(\mathbf{R}) \quad (4)$$

where

$$V_{\mathrm{FVCAS}}(\mathbf{R}) = \sum_{\mathrm{AB}} V^{(2)}_{\mathrm{AB,FVCAS}}(R_{\mathrm{AB}}) + V^{(3)}_{\mathrm{ABC,FVCAS}}(R_{\mathrm{AB}}, R_{\mathrm{BC}}, R_{\mathrm{AC}}) \quad (5)$$

and

$$V_{\mathrm{SEC}}(\mathbf{R}) = \sum_{\mathrm{AB}} V^{(2)}_{\mathrm{AB,SEC}}(R_{\mathrm{AB}}) + V^{(3)}_{\mathrm{ABC,SEC}}(R_{\mathrm{AB}}, R_{\mathrm{BC}}, R_{\mathrm{AC}}) \quad (6)$$

with the first two terms of the SEC series expansion being given by

$$V^{(2)}_{\mathrm{AB,SEC}}(R_{\mathrm{AB}}) = [V^{(2)}_{\mathrm{AB,FVCAS-CISD}}(R_{\mathrm{AB}}) - V^{(2)}_{\mathrm{AB,FVCAS}}(R_{\mathrm{AB}})]/F^{(2)}_{\mathrm{AB}} \quad (7)$$

and

$$V^{(3)}_{\mathrm{ABC,SEC}}(R_{\mathrm{AB}}, R_{\mathrm{BC}}, R_{\mathrm{AC}}) = [V^{(3)}_{\mathrm{ABC,FVCAS-CISD}}(R_{\mathrm{AB}}, R_{\mathrm{BC}}, R_{\mathrm{AC}}) - V^{(3)}_{\mathrm{ABC,FVCAS}}(R_{\mathrm{AB}}, R_{\mathrm{BC}}, R_{\mathrm{AC}})]/F^{(3)}_{\mathrm{ABC}} \quad (8)$$

Note that the summations $\sum_{\mathrm{AB}}$ run only over the correlated diatomic pairs, which can be identified through the dissociation schemes depicted in ref 5.

According to DMBE-SEC[42] method, the two-body scaling parameters $F^{(2)}_{\mathrm{AB}}$ in eq 7 have been chosen to reproduce the bond dissociation energy of the corresponding diatom (AB). At the level of calculation here reported, this leads to $F^{(2)}_{\mathrm{N_2}(^1\Sigma_g^+)} = 0.5491$, $F^{(2)}_{\mathrm{N_2}(^3\Sigma_u^+)} = 0.6408$, $F^{(2)}_{\mathrm{N_2}(^3\Pi_g)} = 0.6359$, and $F^{(2)}_{\mathrm{NH}(^3\Sigma^-)} = 0.8669$. In turn, the three-body factors have been taken to assume identical values for both adiabatic states. Specifically, the value of $F^{(3)}_{\mathrm{ABC}} = 0.823$ has been chosen such as to reproduce the same barrier height for dissociation of the metastable ground-state of HN_2 as the PES reported by Poveda and Varandas[2] which has utilized a larger AV*Q*Z basis set. This result as well as a comparison between the stationary points reported by those authors[2] and the values obtained in the current work is given in Table 1. Despite of the fact that both the resulting global minimum and saddle point for H + N_2 reaction lie below the values reported by Poveda and Varandas[2] by about 0.88 kcal mol^{-1}, the normal-mode frequencies and geometries show considerably smaller deviations. This suggests that the employed scaling factors can compensate for our use of a smaller basis set, at least insofar as the stationary points and thermodynamic attributes are concerned.

We now address the influence of the above correlation scaling in the *ab initio* crossing seams. For the H−N_2 channel, the $R_{\mathrm{H-N_2}}$ coordinate at the crossing point tends to be slightly shifted outward for both T-shaped and linear NHN seams by $\approx 0.15a_0$ when passing from FVCAS to MRCI, and by $\approx 0.05a_0$ in going from MRCI to DMBE-SEC values. In turn, the corresponding energy values also vary. For the equilibrium geometry, $r_{\mathrm{N_2}} = 2.074a_0$, the energy is found to be reduced by ≈30 and ≈20 kcal mol^{-1}, respectively. In the N−NH channel at the linear NHN crossing seam, the $R_{\mathrm{N-NH}}$ coordinate at the crossing is raised by $\approx 0.15a_0$ when passing from FVCAS to MRCI and $\approx 0.05a_0$ when going from MRCI to DMBE-SEC, with the energies for $r_{\mathrm{NH}} = 1.965a_0$ decreasing now by ≈45 and ≈10 kcal mol^{-1}, respectively. The increase in the dynamical correlation has then led to a raising in the perimeter of the structures corresponding to the T-shaped and linear NHN crossing seams.

For the NNH crossing seam, a similar phenomenon occurs, with the perimeter of the triatomic structures at the seam always increasing when adding dynamical correlation. Thus, for a fixed value of *y* in panel b of Figure 1, the inner (left-hand-side) part of the locus has been pushed further inward while the outer (right-hand-side) part has moved outward. Specifically, the inward shifts are typically $\approx 0.15a_0$ and $\approx 0.05a_0$ when passing from FVCAS to MRCI and from MRCI to DMBE-SEC values respectively. The corresponding decreases in energy for $r_{\mathrm{NH}} = 1.965a_0$ are of ≈30 and ≈10 kcal mol^{-1}. As for the outward shifts, such variations are of $\approx 0.1a_0$ and $\approx 0.05a_0$ when going from FVCAS to MRCI and from MRCI to DMBE-SEC values, with the energy for $r_{\mathrm{NH}} = 1.965a_0$ decreasing ≈25 and ≈10 kcal mol^{-1}.

TABLE 1: Stationary Points of the Lower Sheet of the 2 × 2 DMBE Potential Energy Surface

property	MRCI[a]	MRCI[b]	DMBE[c]	DMBE[d]	DMBE[e]
Global Minimum					
R_1/a_0	2.227	2.225	2.226	2.2150	2.226
R_2/a_0	3.586	3.592	3.595	3.590	3.591
R_3/a_0	1.981	1.983	1.983	2.0073	1.982
E/E_h	−0.3568	−0.3582	−0.3568	−0.3583	−0.3582
ΔE[f]	4.59	3.71	4.59	3.65	3.71
ω_1(N−H)/cm^{-1}	2916	2977	2875	2798	3035
ω_2(N−N)/cm^{-1}	1818	1819	1842	1786	1801
ω_3(bend)/cm^{-1}	1118	1130	1096	1357	1125
Saddle Point for H + N_2 Reaction					
R_1/a_0	2.124	2.125	2.125	2.1354	2.121
R_2/a_0	4.135	4.121	4.137	4.241	4.15
R_3/a_0	2.685	2.684	2.688	2.6381	2.712
E/E_h	−0.3399	−0.3413	−0.3399	−0.3414	−0.3413
ΔE[g]	10.62	10.62	10.62	10.62	10.62
ω_1(N−H)/cm^{-1}	1619*i*	1575*i*	1624*i*	1580*i*	1496*i*
ω_2(N−N)/cm^{-1}	2155	2167	2104	2095	2097
ω_3(bend)/cm^{-1}	762	755	778	783	834
Saddle Point for H−N_2 Isomerization					
R_1/a_0	2.324	2.309	2.326	2.331	2.299
R_2/a_0	2.285	2.312	2.281	2.262	2.265
R_3/a_0	2.285	2.312	2.281	2.2624	2.265
E/E_h	−0.2867	−0.2866	−0.2868	−0.2768	−0.2866
ΔE[g]	44.05	45.00	43.99	51.22	45.00
ω_1(N − H)/cm^{-1}	2676	2604	2753	2311	2845
ω_2(N−N)/cm^{-1}	1660	1707	1671	1601	1766
ω_3(bend)/cm^{-1}	2278*i*	2314*i*	2275*i*	1921*i*	1771*i*

[a] Reference 2, from a fit to a Taylor-series expansion around the stationary point. [b] This work, from a fit to a Taylor-series expansion around the stationary point; see the text. [c] Single-sheeted representation from ref 2. [d] This work using preliminary estimate for coupled states; see the text. [e] This work, final PES; see the text. [f] Relative to H + N_2 asymptote (in kcal mol^{-1}). [g] Relative to the corresponding global minimum (in kcal mol^{-1}).

4. The Diabatization Procedure

As discussed in section 2, approaches based on molecular properties could offer the advantage of obtaining at low cost[38] the diabatization angle, which could therefore be used for generating zeroth-order solutions of the diabatic matrix. This was the approach that we have first followed. We start by noting that the $1^2A''$ state of HN_2 is related with the second and third $^2A'$ states of the title system, and hence the use of the transition dipole moment as an auxiliary diabatization property would involve at least four states. Thus, we tried to use instead the dipole moment, following previous work on a double-sheeted DMBE PES for C_2H.[9] However, the implementation of this procedure for HN_2 revealed itself quite cumbersome. As for H_2O,[38] the definition of the axis along which the component of

the dipole moment vector better describes the avoided crossing is not the same for every conical intersection of HN_2, with obvious inconsistencies arising between the diabatic points generated from distinct choices of optimal directions. We have then adopted the criterion of Dobbyn and Knowles[38] for choosing the optimum orientation of the dipole moment. Unfortunately, many profiles obtained in this way failed to show the correct atom−diatom dissociation behavior, with spurious intersections (diabatization angle equal to $\pi/4$) even arising in regions of relevance for the modeling. Such difficulties appeared in particular for the N−NH channel where close to NNH linearity, two conical intersections must be reproduced while, for NHN arrangements, only one is present. Although the results for each channel could be handled to produce acceptable results, serious difficulties arose when merging them all to get global diabatic sheets.

A new diabatization scheme had to be envisaged to obtain a satisfactory global form for the diabatization angle. Although not essential, we would like it to be simple and analytic. It should also make unnecessary the use of *ad hoc* local modifications,[9,38,48,58] which might add further inconsistencies in the diabatic data in addition to those caused by coupling of the target states with higher excited ones.[5,49] In addition, a well-defined behavior at all atom−diatom channels is mandatory. This does not appear to have been given in early studies,[48,50,51] as judged from the resulting diabats and adiabats,[50,51] or by the fact that it does not contemplate all channels.[48] Finally, the form employed should allow the diabatization angle to describe all crossing seams to their full extend.

The algebraic form that we have envisaged to represent the diabatization angle is

$$\alpha(\mathbf{R}) = f(\alpha_{H-N_2}, \alpha_{N-NH}) \tag{9}$$

where α_{H-N_2} and α_{N-NH} are diabatization angles designed to individually describe the H−N_2 and N−NH channels, respectively. This would allow one to reduce the 4*D* problem to two 3*D* problems. Such a scheme has proved to be sufficiently realistic for HN_2, as will be clear in the following. Such a separability has been further explored by the use of a product form for $f(\alpha_{H-N_2}, \alpha_{N-NH})$, namely

$$\alpha(\mathbf{R}) = \alpha_{H-N_2}(\mathbf{R})\alpha_{N-NH}(\mathbf{R}) \tag{10}$$

The first property one seeks for such forms is that α_{H-N_2} and α_{N-NH} vanish at the corresponding asymptotic channels, as imposed by the calculated data that indicate the nonexistence of crossing seams at asymptotic atom−diatom distances.[5] By further exploring the topology of the crossings and avoided intersections, we have collected the latter points shown in Figure 2 (these have been determined by searching for the smallest energy gap along rays corresponding to fixed atom−diatom Jacobi angles) with the requirement that they should evolve to the corresponding crossing seams at the boundaries (of C_{2v}, $C_{\infty v}$, or $D_{\infty v}$ symmetry, for each value of the BC bond distance). This led us to the existence of two surfaces of avoided intersections, one for each individual channel. With $R^0_{H-N_2}(r_1, \theta_1)$ and $R^0_{N-NH,2}(r_2, \theta_2)$ being the analytic representations of such surfaces for the H−N_2 and N−NH channels, a convenient representation is

$$\alpha_{H-N_2}(\mathbf{R}) = \frac{1}{2}\{1 - \tanh[\gamma_1(R_{H-N_2} - R^0_{H-N_2})]\} \tag{11}$$

for the channel H−N_2, and

$$\alpha_{N-NH}(\mathbf{R}) = \alpha'_{N-NH,2}(\mathbf{R})\alpha'_{N-NH,3}(\mathbf{R}) \tag{12}$$

for the channel N−NH, with

$$\alpha'_{N-NH,2}(\mathbf{R}) = \frac{1}{2}\{1 - \tanh[\gamma_2(R_{N-NH,2} - R^0_{N-NH,2})]\} \tag{13}$$

Note that the product in eq 12 insures the correct permutational symmetry (N atoms denoted by 2 and 3). Note further that $R^0_{H-N_2}$ provides a single piece of data for any coordinate-pair (r_1, θ_1) in C_s symmetry where the argument in eq 11 vanishes and thus $\alpha_{H-N_2}(\mathbf{R}) = 0.5$. For larger or smaller values of R_{H-N_2}, eq 11 yields $\alpha_{H-N_2}(\mathbf{R}) \rightarrow 0$ and $\alpha_{H-N_2}(\mathbf{R}) \rightarrow 1$. The same holds for the N−NH channel by eq 13.

The simplest representation of $R^0_{H-N_2}(r_1, \theta_1)$ and $R^0_{N-NH,2}(r_2, \theta_2)$ is motivated by the interpretation of the symmetry allowed crossing seams of C_{2v} and $C_{\infty v}$ symmetry as boundary curves. For the channel H−N_2, that would be

$$R^0_{H-N_2}(r_1, \theta_1) = R^{nnh}_{H-N_2}(r_1)d(2\theta_1) + R^T_{H-N_2}(r_1)[1 - d(2\theta_1)] \tag{14}$$

where $d(\theta)$ is the damping function $d(\theta) = 0.5[1 + \cos(\theta)]$, which makes $R^{nnh}_{H-N_2}$ vanish for C_{2v} arrangements (denoted by the index *T*) where $\theta_1 = 90°$, and $R^T_{H-N_2}$ for NNH linear arrangements where $\theta_1 = 0°$. In turn, for the N−NH channel, we write

$$R^0_{N-NH,2}(r_2, \theta_2) = R^{nhn}_{N-NH}(r_2)d(\theta_2) + R^{hnn}_{N-NH}(r_2)[1 - d(\theta_2)] \tag{15}$$

with $d(\theta)$ as in eq 14, now annihilating R^{hnn}_{N-NH} for NHN linear arrangements where $\theta_2 = 0°$, and R^{nhn}_{N-NH} for NNH linear arrangements where $\theta_2 = 180°$. The functions $R^{nnh}_{H-N_2}$, $R^T_{H-N_2}$, R^{nhn}_{N-NH}, and R^{hnn}_{N-NH} in eqs 14 and 15, which represent the Jacobi coordinate at the crossing points along the seams indicated by the superscripts (heavy solid lines in Figure 2), have been obtained by fitting the DMBE-SEC points described in section 3. We have first written for the H−N_2 channel

$$R^T_{H-N_2}(r_1) = y_T(r_1) \text{ and } R^{nnh}_{H-N_2}(r_1) = y_{nnh}(r_1) + \frac{r_1}{2} \tag{16}$$

where y_T is the Jacobi distance between the H atom and the center of the diatom N_2 along the C_{2v} crossing seam, as a function of the NN bond distance r_1. In turn, y_{nnh} is the bond distance NH along the NNH crossing seam, also represented as a function of r_1. Finally, we considered for the N−NH channel

$$R^{hnn}_{N-NH}(r_2) = y_{hnn}(r_2) + \frac{r_2}{2} \text{ and } R^{nhn}_{N-NH}(r_2) = y_{nhn}(r_2) + \frac{r_2}{2} \tag{17}$$

where y_{nhn} is the HN distance as a function of the NH distance r_2 along the linear NHN crossing seam and y_{hnn} is the bond distance NN, also as a function of the r_2.

To model y_T, we have chosen the form

$$y_T(r_1) = a_T[r_1 + b_T r_1^3 \exp(-\alpha_T r_1)]\{1 + \tanh[\beta_T(r_1 - r_T)]\} \quad (18)$$

such that y_T asymptotically raises up to atomization as a linear function of r_1, which would reproduce the most likely scenario for such kind of crossing seam.[5] Note that we have chosen $y_T(r_1)$ such as to assume very small values for $r_1 \lesssim 1.5a_0$, where no data is available. For y_{nnh}, we have considered

$$y_{nnh}(r_1) = a_{nnh} \exp(c_{nnh,1}\Delta r_{nnh,1} - c_{nnh,2}\Delta r_{nnh,2}^2 - c_{nnh,8}\Delta r_{nnh,8}^8) \quad (19)$$

where $\Delta r_{nnh,i} = r_1 - r_{nnh,i}$, which has been designed to reproduce simultaneously the shape of NH as a function of r_1 in the interval $1.5 \lesssim r_1/a_0 \lesssim 3.6$ as well as the rapid decay for both small ($r_1 \lesssim 1.5a_0$) and large ($r_1 \gtrsim 3.6a_0$) values of this coordinate. In turn, the functional form y_{nhn} was chosen as

$$y_{nhn}(r_2) = a_{nhn,1}T[s_{nhn,11}(r_2 - r_{nhn,11}) + s_{nhn,12}(r_2 - r_{nhn,12})] + a_{nhn,2}T[s_{nhn,21}(r_2 - r_{nhn,21})] + a_{nhn,3}T[s_{nhn,31}(r_2 - r_{nhn,31})] \quad (20)$$

with $T(x) = 1 - \tanh(x)$. This functional form have been adopted such that for $r_2 = 0$ we have a finite value for y_{nhn}, while for $r_2 \geq 2.5a_0$ one would have y_{nhn} assuming very small values. To model the avoided intersections for the N−NH channel, we require the NNH crossing seam specifically for this channel as indicated in eqs 17, having chosen the form

$$y_{hnn}(r_2) = a_{hnn}\{1 - \tanh[s_{hnn,1}(r_2 - r_{hnn,1}) + s_{hnn,2}(r_2 - r_{hnn,2})]\} \quad (21)$$

Naturally, the NNH crossing seam could not be fully represented by a single valued expression like eq 21 as discussed in ref 5, since for a value of the NH bond distance we have two NNH conical intersections whenever $r_{NH} \lesssim 2.9a_0$. We have chosen to parametrize this function by focusing for each NH separation on the conical intersection closer to the N + NH limit. Thus, y_{hnn} has been made to assume small values for $r_2 \gtrsim 3.0a_0$, while fitting the conical intersection for $r_2 \lesssim 3.0a_0$ and assume a constant value at $r_2 \to 0$. The optimum parameters in eqs 18−21 are given in Table 1 of the Supporting Information.

Some small adjustments turned out necessary to improve eqs 14 and 15. For $R^0_{H-N_2}$, a maximum arising in the radial value for the avoided intersections at intermediate values of the Jacobi angle (see panel **a**) has been mimicked by adding

$$p_1(r_1, \theta_1) = (a_0 + a_2\Delta\theta_1^2 + a_4\Delta\theta_1^4) \exp(\gamma_1\Delta r_1 - \gamma_2\Delta r_1^2) \quad (22)$$

to eq 14, where $\Delta\theta_1 = \theta_1 - \theta_1^0$, and $\Delta r_1 = r_1 - r_1^0$. The parameters in eq 22 have been fitted to the points shown in panel **a** of Figure 2 by using the form

$$R^0_{H-N_2}(r_1, \theta_1) = R^{nnh}_{H-N_2}(r_1)d(2\theta_1) + R^T_{H-N_2}(r_1)[1 - d(2\theta_1)] + p(r_1, \theta_1)\sin^2(2\theta_1) \quad (23)$$

Although a satisfactory fit to the points shown in panel **b** of Figure 2 has been achieved, a small inaccuracy has appeared near T-shaped geometries by using the simple product in eq 12. This has been corrected by adding to eq 15 the form

$$p_2(r_2, \theta_2) = (a_0 + a_1\Delta\theta_2)^2 \exp(-\alpha\Delta\theta_2^2) + a_3 r_2[1 + \tanh(\gamma\Delta r_2)] \quad (24)$$

where $\Delta\theta_2 = \theta_2 - \theta_2^0$, and $\Delta r_2 = r_2 - r_2^0$. The function $R^0_{N-NH,2}$ is now defined as

$$R^0_{N-NH,2}(r_2, \theta_2) = R^{nhn}_{N-NH}(r_2)d(\theta_2) + R^{hnn}_{N-NH}(r_2)[1 - d(\theta_2)] + p_2(r_2, \theta_2)\sin^2(\theta_2) \quad (25)$$

The parameters in eqs 22 and 24 are given in Table 1 of the Supporting Information.

Panels **a** and **b** of Figure 1 show the crossing seams predicted by eq 11. As expected, this form gives by construction a correct description of the C_{2v} and linear NNH crossing seams. We have then proceeded with the diabatization using only eq 11, which has revealed that the topology of the avoided intersections is correctly described for the H−N_2 channel over the whole range of calculated points. No unpleasant features have been noted at regions uncovered by the *ab initio* data in this channel. In fact, it has even partly proved to predict the crossing and avoided crossing at the N−NH channel for linear NNH arrangements.

As for the H−N_2 channel, a direct check of the predicted crossing seams via eq 13 would give an excellent agreement with the points that have been used for fitting the boundary curves in eqs 20 and 21, but the situation at the N−NH channel would not be so simple as we have also to ensure under the N atom permutation via eq 12. Figure 1 shows the crossing seam predictions using eq 25 and eq 12. It is seen from panel **a** that such a product predicts the $D_{\infty h}$ conical intersection, although slightly displaced from the *ab initio* prediction. Moreover, it predicts the crossing of the diabatic states that evolves into such a $D_{\infty h}$ conical intersection. Panel **b** shows the predicted linear NNH crossing seam, which reproduces the *ab initio* crossing seam but for $x \lesssim 2.5a_0$, which might be expected from our choice of eq 21. Panel **c** shows that the predicted linear NHN crossing seam is only slightly shifted from the *ab initio* locus in accordance with the small shift observed for the $D_{\infty h}$ conical intersection in panel **a**. We have diabatized the adiabatic states using the product in eq 12, with quite satisfactory results for the N−NH channel. For each NH bond distance, the crossing of the diabatic states is found to evolve smoothly with θ_{N-NH} from the linear NHN conical intersection to the conical intersection closest to the atom−diatom limit at NNH linear arrangements. In addition, we observe the correct merging of the diabatic states with the adiabatic ones at the N−NH atom−diatom limit.

Figure 1 further shows that the only significant deviations observed in the crossing seams predicted by using the global diabatization angle in eq 10 is observed for the linear NNH arrangements in panel **b**. However, the resulting diabatic profiles, depicted for the most representative geometries ($1.8 < r_{N_2}/a_0 < 3.3$ and $2.465 < r_{NH}/a_0 < 3.365$) in Figures 3 and 4 show themselves to mimic correctly the *ab initio* trends when evolving from the C_{2v} to linear arrangements (for the H−N_2 channel) as well as for linear NNH and NHN. Therefore, such deviations are expected to be irrelevant for modeling purposes. In addition, Figures 3 and 4 reveal that the global structure of the crossing-seams is in fact recovered by the diabatic states. This can be seen from panel **i** of Figure 3 that shows the

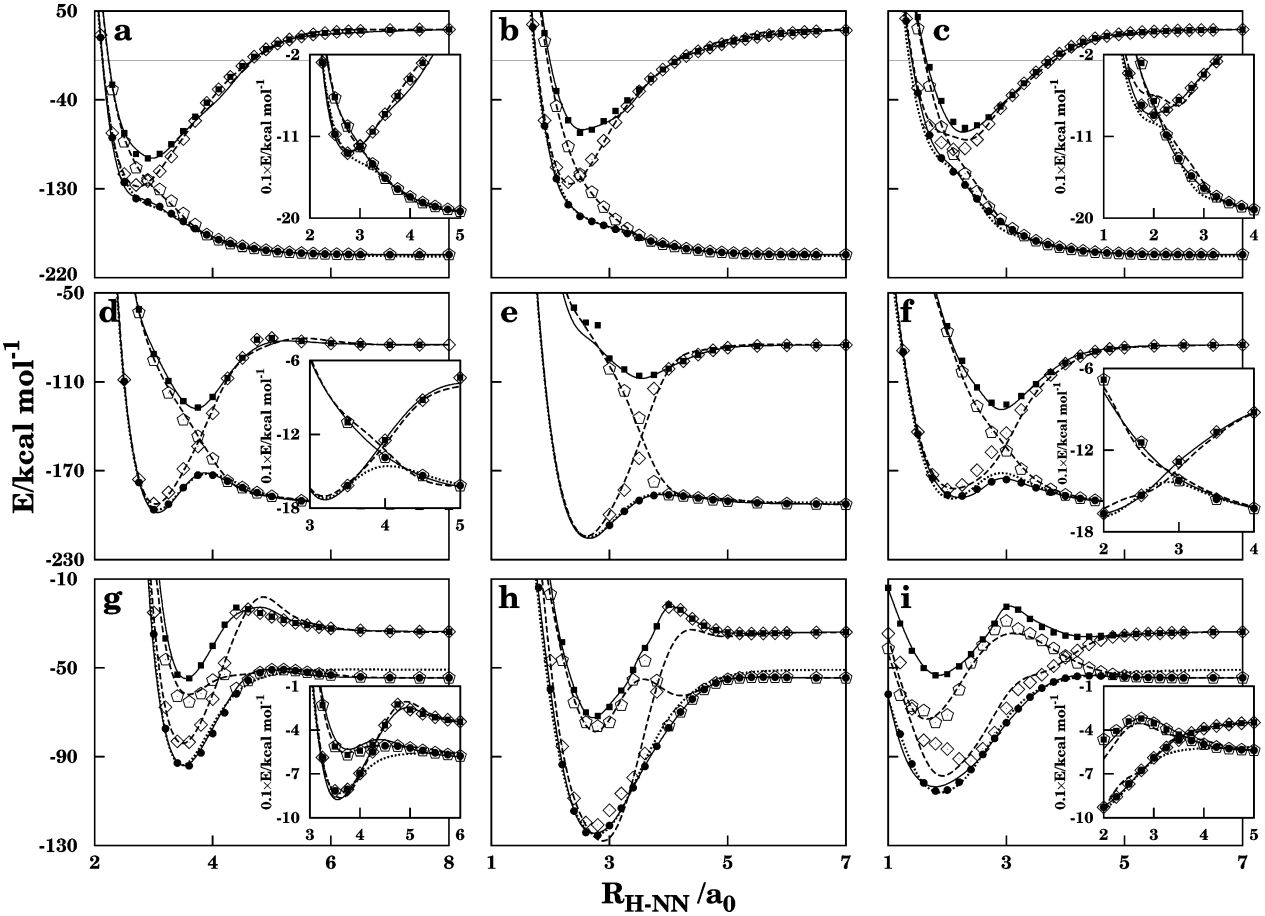

Figure 3. Adiabatic profiles and *ab initio* energies for the H−NN channel. The first row of panels and insets refer to $r_{N_2} = 1.854a_0$, the second to $2.574a_0$, and the third to $3.074a_0$. The angle θ in first column of panels is 15°, in the second 45°, and in the third 75°. The insets in the first column correspond to HNN linear arrangements ($\theta = 0°$), and in the third column to T-shaped arrangements ($\theta = 90°$). Key for symbols: (●) $1^2A'$; (■) $2^2A'$; (⌂) V_{11}; (◇), V_{22}; (—) adiabatic states; (− −) diabatic states; (---) PES for the $1^2A'$ state from ref 2.

increasing influence of the $D_{\infty h}$ conical intersection in the diabatic states as r_{N_2} increases to approach the value of $\approx 3.7a_0$. Additionally, Figure 4 shows that despite the intersection of the diabatic states for C_s arrangements at $r_{NH} \gtrsim 2.8a_0$, such an intersection smoothly disappears when approaching the NNH and NHN linear arrangements as it should be from Figure 1.

Finally, we note that the diagonal diabatic states V_{11} and V_{22} merge into the corresponding adiabatic states V^- and V^+ for both channels as shown in Figures 3 and 4 when the off-diagonal term V_{12} becomes vanishingly small. Thus, the diabatic states generated from the relations

$$V_{11}(\mathbf{R}) = V^+(\mathbf{R}) \sin^2 \alpha(\mathbf{R}) + V^-(\mathbf{R}) \cos^2 \alpha(\mathbf{R})$$
$$V_{22}(\mathbf{R}) = V^+(\mathbf{R}) \cos^2 \alpha(\mathbf{R}) + V^-(\mathbf{R}) \sin^2 \alpha(\mathbf{R})$$
$$V_{12}(\mathbf{R}) = [V^+(\mathbf{R}) - V^-(\mathbf{R})] \sin \alpha(\mathbf{R}) \cos \alpha(\mathbf{R}) \quad (26)$$

employing the diabatization angle in eq 10 not only account for the crossing seams/avoided intersection topology but also fulfill the asymptotic relations

$$\lim_{\substack{R_{H-N_2}\to\infty \\ \text{or } R_{N-NH}\to\infty}} \begin{pmatrix} V_{22} & V_{12} \\ V_{12} & V_{11} \end{pmatrix} = \begin{pmatrix} V^+ & 0 \\ 0 & V^- \end{pmatrix} \quad (27)$$

at both the H + N_2 and N + NH atom−diatom dissociation limits.

5. Modeling of Diabatic States

5.1. Outline of 2 × 2 Diabatic DMBE Matrix. A primary step on the expansion of the diagonal diabatic states in DMBE theory is the formulation of the relevant dissociation scheme. For V_{11}, one has[2]

$$V_{11} \to \begin{cases} N_2(^1\Sigma_g^+) + H(^2S) \\ NH(^3\Sigma^-) + N(^4S) \end{cases} \quad (28)$$

For V_{22}, correlated at dissociation with the first excited adiabatic state, we write

$$V_{22} \to \begin{cases} N_2(^3\Pi_g)k(x) + N_2(^3\Sigma_u^+)[1 - k(x)] + H(^2S) \\ N(^2D)F(\mathbf{R}) + NH(^3\Sigma^-) \end{cases} \quad (29)$$

where $k(x)$, and $F(\mathbf{R})$ are auxiliary functions to be defined below. In turn, the crossed diabatic state is chosen such that $V_{12} \to 0$ for any dissociation channel.

In a previous study, we have shown[5] that the first two excited states of the $HN_2(^2A')$ manifold are strongly coupled showing at least two seams of conical intersections, one for T-shaped geometries, the other for collinear ones. Concerning atom plus diatom dissociation, it has also been shown that the linear $2^2A'/3^2A'$ seam imposes strong correlation between the involved states. Thus, for reducing this multistate problem into a two-state one, one needs to treat them as narrowly avoided crossings.

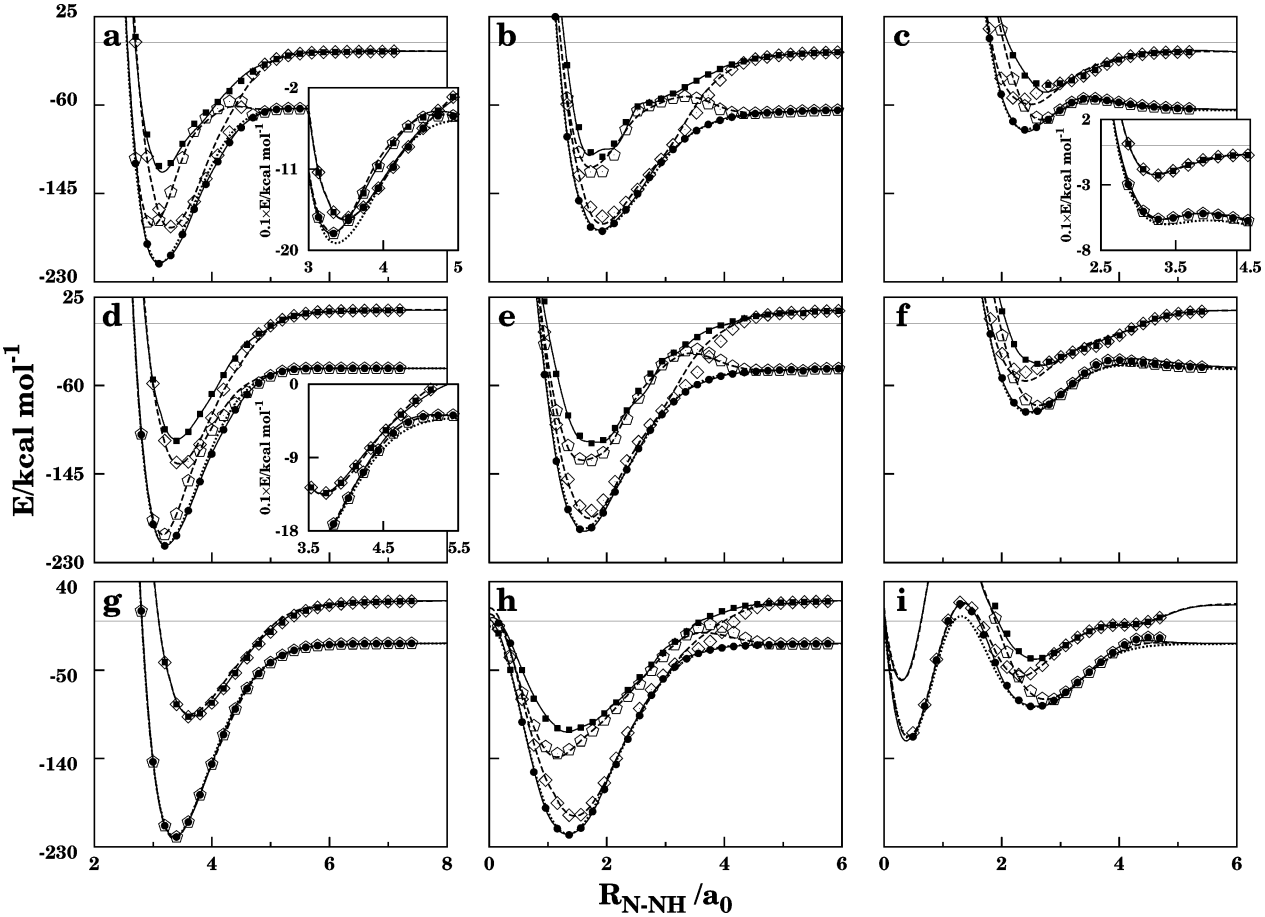

Figure 4. Adiabatic profiles and *ab initio* energies for the N−NH channel. For the first row of panels and insets we have fixed r_{NH} at $2.465a_0$, for the second row at $2.865a_0$ and for the third at $3.365a_0$. In the first column of panels, $\theta = 150°$, in the second 90°, and in the third 45°. The insets in the first column correspond to HNN linear arrangements ($\theta = 180°$) and in the third to NHN linear arrangements ($\theta = 0°$). Key for symbols is as given in Figure 3.

For this purpose, we observe that at the H−N_2 dissociation the first excited-state behaves differently for $0 < r_{N_2}/a_0 \lesssim 1.95$ and $1.95 \lesssim r_{N_2}/a_0$. As suggested in eq 29, this can be modeled via a one-dimensional (1*D*) switching function $k(x)$. This function becomes unity for the interval $0 < r_{N_2}/a_0 \lesssim 1.95$ and vanishes for $1.95 \lesssim r_{N_2}/a_0$, varying continuously but drastically between those intervals. This will preserve the correct atom plus diatom behavior on each interval and simultaneously provides a simple mathematical structure to pass from one region to the other. As shown in eq 30 for the N−NH dissociation, a 3*D* switching function $F(\mathbf{R})$ must be employed to connect the intervals $0 < r_{NH}/a_0 \lesssim 3.0$ and $3.0 \lesssim r_{NH}/a_0$.

Given the asymptotic limits on eq 28, the DMBE expansion for the diabatic state V_{11} will assume the form

$$V_{11}(\mathbf{R}) = V_{11}^{(3)}(\mathbf{R}) + N_2(^1\Sigma_g^+)(R_1) + NH(^3\Sigma^-)(R_2) + NH(^3\Sigma^-)(R_3) \quad (30)$$

where $V_{11}^{(3)}(\mathbf{R})$ and the diatomic potentials, as usually done in DMBE theory, are analytically split into their extended Hartree−Fock and dynamical correlation components:

$$V^{(n)}(\mathbf{R}) = V_{EHF}^{(n)}(\mathbf{R}) + V_{dc}^{(n)}(\mathbf{R}) \quad (31)$$

with $n \geq 2$. Since $2N(^4S) + H(^2S)$ is taken as the energy reference, no one-body energy terms will arise in V_{11}. In fact, the DMBE expansion in eq 30 has the form employed for the ground state of HN_2.[2]

The asymptotic limits for V_{22} in eq 29 will be warranted by writing

$$V_{22}(\mathbf{R}) = V_{22}^{(3)}(\mathbf{R}) + N_2(^3\Pi_g)(R_1)k(R_1) + N_2(^3\Sigma_u^+)(R_1)\,[1 - k(R_1)] + NH(^3\Sigma^-)(R_2) + NH(^3\Sigma^-)(R_3) + [N(^2D) - N(^4S)]F(\mathbf{R}) \quad (32)$$

where the two- and three-body terms are constructed as in eq 31, and the difference $N(^2D) - N(^4S)$ accounts for the $N(^2D)$ one-body energy. According to DMBE theory, the $V_{EHF}^{(n)}(\mathbf{R})$ terms are constructed to vanish at the asymptotes whenever one of the atoms is removed from the cluster, while $V_{dc}^{(n)}(\mathbf{R})$ is semiempirically modeled to describe the atom plus diatom dynamical correlation. It is then clear that the diabatic state $V_{11}(\mathbf{R})$ will respect the scheme in eq 28, with the same applying to $V_{22}(\mathbf{R})$ and the scheme in eq 29 provided that $F(\mathbf{R})$ in eq 32 is suitably designed for this matter.

Besides the correct asymptotic description, the diabatic states must be designed such as to provide a correct description of the conical intersections involving the corresponding adiabatic states. Since the diagonal diabatic states are decoupled at the neighborhood of the conical intersections, no further constraints are required in eqs 30 and 32. The off-diagonal diabatic state must, however, vanish at the crossing seams. In addition, it must satisfy $V_{12} \rightarrow 0$ whenever any bond distance goes to infinity. We have chosen for this purpose the form

$$V_{12}(\mathbf{R}) = V^{(3)}_{12,\mathrm{EHF}}(\mathbf{R}) f_l(\mathbf{R}) f_T(\mathbf{R}) \tag{33}$$

where the extended Hartree−Fock term in eq 33 has a similar form as for the diagonal diabatic terms, which makes $V_{12}(\mathbf{R})$ vanish at any dissociation asymptote. To make V_{12} vanish at the linear (l) and C_{2v} (indexed by T) crossing seams, one uses the functions $f_l(\mathbf{R})$ and $f_T(\mathbf{R})$. For the former, we use

$$f_l(\mathbf{R}) = \sin \theta_{\mathrm{NHN}} \tag{34}$$

where θ_{NHN} is the included angle ∠NHN, thus making V_{12} vanish at both NNH and NHN linear arrangements. For the C_{2v} geometries, no simple form has shown to be appropriate. In fact, the topology of the problem has forced us to employ a nonanalytical form as described later.

5.2. The Switching Function *F*(R). When restricting the multistate problem to a two-state one via eq 32, we will be dealing with a problem similar to the one dealt by Varandas and Poveda[71] when obtaining a single valued representation of the NH_2 PES. To accurately model a narrowly avoided crossing at the N−H_2 dissociative channel, they proposed the switching form

$$f(\mathbf{R}) = g(r_1) h(R_1) \tag{35}$$

where R_1 is the distance between the hydrogen atoms and r_1 the Jacobi coordinate separating the atom N from the geometric center of the diatom H_2. Such an approach offers a more realistic treatment over the one suggested by Murrell and Carter[72] for obtaining a single-sheeted form for the water molecule. The function $h(R_1)$ is calibrated from scaled *ab initio* calculations on the fragments in order to control the $N(^2D) - N(^4S)$ decay, while $g(r_1)$ is used to mimic the energy difference $N(^2D) - N(^4S)$ when approaching intermediate interactions in the triatom. With their approach, Varandas and Poveda[71] not only obtained a smoother behavior at all configuration space but also overcame the well-known failures of the earlier Murrell−Carter approach.[72]

For the N−NH channel of $HN_2(2^2A')$, we must deal with the $N(^2D) - N(^4S)$ decay of two nitrogen atoms, and the required symmetrization. This has been achieved with

$$F'(\mathbf{R}) = g(r_2) h(R_2) + g(r_3) h(R_3) \tag{36}$$

where the same notation as for NH_2[71] has been employed. Thus, if the indexes (i, j, k) number the atoms (1 for H; 2 and 3 for N), r_i represents the Jacobi coordinate separating atom i from the geometric center of diatom jk, whose internuclear distance is denoted by R_i. Note that $F'(\mathbf{R})$ ensures not only symmetrization, but also the requirements to be fulfilled by $f(\mathbf{R})$ in eq 35. Both functions $h(R_i)$ and $g(r_i)$ assume similar functional forms as for NH_2, namely

$$h(R_i) = \{1 - \tanh[\alpha_1(R_i - R_0^1) + \alpha_2(R_i - R_0^2)^5]\} \tag{37}$$

and

$$g(r_i) = \frac{1}{2}\{1 + \tanh[\alpha(r_i - r_1^0)]\} \tag{38}$$

The inset of panel **a** of Figure 5 shows the result of the least-squares fit of $h(R_i)$, with $N(^2D)$ lying 0.08920979 E_h above $N(^4S)$. The resulting parameters are: $\alpha_1 = 0.995366 a_0^{-1}$, $\alpha_2 = 0.165409 a_0^{-1}$, $R_0^1 = 3.49359 a_0$, and $R_0^2 = 4.60365 a_0$. In turn, the parameters in $g(r_i)$ are $\alpha = 1.5 a_0^{-1}$ and $r_0 = 5.0 a_0$, having been chosen to ensure smoothness. As detailed in the subtitles of Figure 5, we have considered two sets of *ab initio* points in the fit, mainly due to the impossibility of covering the R_1 distance up to sufficiently large values.[5] The triatom scaled *ab initio* points correspond to the (○) set of points in panel **a** of Figure 5. Despite our effort to obtain a trend of *ab initio* points as smooth as possible, such results were always influenced by the strong couplings with higher excited states, and thus modeling $h(R_i)$ as accurately as for the ground state of NH_2[71] was out of the question. The second set of points, indicated by (□), corresponds to *ab initio* calculations in the diatomic state $NH(^5\Sigma)$, and were included to ensure a realistic description where the triatomic averaged state calculations did not converge. A rmsd below 0.9 kcal mol has been obtained.

Finally, linear NHN plots of $F'(\mathbf{R})$ for fixed NH reveal a barrier above 1 with a maximum at the $D_{\infty h}$ configurations, which grows with the NH separation. Since we have *ab initio* points covering this region, the three body terms in eq 32 would be expected to compensate such a barrier if so required. However, such a barrier arises at configurations far from equilibrium which would be difficult to model with the extended HF term (see eq 47). To overcome this difficulty, we have used the function

$$F(\mathbf{R}) = F'(\mathbf{R})(R_2 - R_3)^2 \tag{39}$$

which keeps all the prescribed attributes of $F'(\mathbf{R})$.

5.3. Two-Body Terms and One-Dimensional Switching Function *k*(*x*). The diatomic potential curves $N_2(^1\Sigma_g^+)$, $N_2(^3\Sigma_u^+)$ and $NH(^3\Sigma^-)$ have been modeled using the extended Hartree−Fock approximate correlation energy method for diatomic molecules including the united atom limit[73] (EHFACE2U), with the available parameters being determined by fitting *ab initio* data. The dynamical correlation ("long-range") part assumes the form[74]

$$V_{\mathrm{dc}}(R) = -\sum_{n=6,8,10} \chi_n(R) \frac{C_n}{R^n} \tag{40}$$

where $\chi_n(R)$ are damping functions $\chi_n(R) = [1 - \exp(-A_n R/\rho - B_n R^2/\rho^2)]^n$, and A_n and B_n are the auxiliary functions $A_n = \alpha_0 n^{-\alpha_1}$ and $B_n = \beta_0 \exp(-\beta_1 n)$; the "universal" dimensionless parameters for all isotropic interactions[12,13] are $\alpha_0 = 16.36606$, $\alpha_1 = 0.70172$, $\beta_0 = 17.19338$, and $\beta_1 = 0.09574$. In turn, the scaling parameter is defined by $\rho = 5.5 + 1.25 R_0$, with $R_0 = 2[\langle r_A^2\rangle^{1/2} + \langle r_B^2\rangle^{1/2}]$ determining[75] the onset of the undamped R^{-n} expansion, and $\langle r_X^2\rangle$ the expectation value of the squared radius for the outermost electrons of atom X(=A, B). The EHF-type energy term assumes the general form

$$V_{\mathrm{EHF}}(R) = -\frac{D}{R}\left(1 + \sum_{i=1}^{n} a_i r^i\right) \exp(-\gamma r) \tag{41}$$

where $\gamma = \gamma_0[1 + \gamma_1 \tanh(\gamma_2 r)]$, $r = R - R_e$ is the displacement from the equilibrium diatomic geometry, and D and $a_i (i = 1, ..., n)$ are adjustable parameters.[13,73] For our purposes, it was sufficient to calibrate the potential curves of these diatomic potentials exclusively from the DMBE-SEC points described in section 3. A rmsd of 5 cm^{-1} has been achieved for all diatomics except $N_2(^3\Pi_g)$. All curves are displayed in Figure 5. The agreement with the more accurate results of ref 2 for $N_2(^1\Sigma_g^+)$ and $NH(^3\Sigma^-)$ is in the milihartree range, which is likely to be within the accuracy of their own data.[76]

For $N_2(^3\Pi_g)$, a carefull analysis of the *ab initio* data has shown an unexpected non-trivial behavior at dissociation. At the

FVCAS level, a barrier of ≈1315 cm^{-1} above dissociation arises at $R_{NH} \approx 4.2a_0$. However, it becomes ≈340 cm^{-1} at $R_{NH} \approx 4.5a_0$ when using the MRCI method, but now lying ≈77 cm^{-1} below dissociation. After DMBE-SEC scaling (see section 3), such a barrier is further reduced to ≈43 cm^{-1}, now at $R_{NH} \approx 4.8a_0$ but ≈200 cm^{-1} below dissociation; see the upper inset in panel **b** of Figure 5. Note that we have repeated these calculations with the AV*Q*Z basis, and the same pattern has been observed. In an attempt to rationalize this barrier we have performed *ab initio* calculations for the excited states of this same symmetry looking for the possibility of such barrier to correspond to an avoided crossing. This could not be confirmed, thus establishing a pattern similar to that for[77,78] $CO(^1\Pi)$.

To model $N_2(^3\Pi_g)$, we recalled previous work for $CO(^1\Pi)$, where it was suggested[79] that the above barrier could be understood as a consequence of the repulsive behavior of the asymptotic exchange energy. It has been written as

$$V_{EHF}(R) = -\frac{D}{R}(1 + \sum_{i=1}^{n} a_i r^i)\exp(-\gamma r) + V_{exc}^{asym}(R)\chi_{exc}(R) \quad (42)$$

where the asymptotic exchange contribution has been made explicit. For CO, this term has been shown[79] to assume the form

$$V_{exc}^{asym}(R) = (\alpha_{exc}R^2 - \beta_{exc}R)R^{1/2}\exp(-\sigma_{exc}R) \quad (43)$$

where α_{exc}, β_{exc}, and σ_{exc} are parameters; the damping function $\chi_{exc}(R)$ assumes the form of $\chi_5(R)$ defined previously for the dynamical correlation; for further details, see the original papers.[78,79] Instead of calculating the matrix elements of the asymptotic exchange contribution, we have pragmatically determined α_{exc}, β_{exc}, and σ_{exc} in eq 43 via a least-squares fit of the EHF points at the neighborhood of the barrier. These points were obtained as the difference between the DMBE-SEC points and the semiempirical dynamical correlation contribution in eq 40, with the parameters written in Table 2 of the Supporting Information. Also in this table are the parameters obtained by a linear least-squares fit to the EHF energies, which were obtained by subtracting the asymptotic exchange contribution plus the semiempirical dynamical correlation from the DMBE-SEC points. A rmsd smaller than 2.5 cm^{-1} has been obtained close to the equilibrium distance and the barrier; its value is around 8.0 cm^{-1} for the whole curve, which is plotted in panel **b** of Figure 5.

After modeling the diatomic curves, we turned to fitting the 1*D* switching function $k(x)$ by using the form

$$k(x) = 0.5\{1 + \tanh[\sigma(x - x_0)]\} \quad (44)$$

with σ and x_0 being fitted via the form $N_2(^3\Pi_g)k(x) + N_2(^3\Sigma_u^+)[1 - k(x)]$ (see eq 32) to the black points in panel **b** of Figure 5; all diatomic parameters were kept fixed at the values obtained when modeling the respective diatomic states. The values $\sigma = 48.2379a_0^{-1}$ and $x_0 = 2.01950a_0$ were obtained, with the rmsd being 5 cm^{-1}. As seen from the lower inset in panel **b** of Figure 5, the intersection between the diatomic curves is avoided smoothly.

5.4. Three-Body Dynamical Correlation Energy. For the three-body dynamical correlation, we have used the semiempirical form[80]

$$V_{dc}^{(3)} = -\sum_i \sum_n g_i(\mathbf{R})C_n^{(i)}(R_i, \theta_i)\chi_n(r_i)r_i^{-n} \quad (45)$$

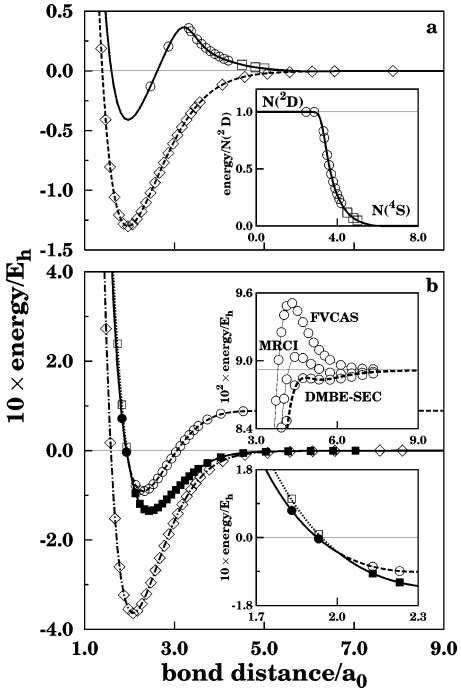

Figure 5. EHFACE2U potentials energy curves. Key for panel **a**: (○) $HN_2(2^2A')$ with r_{NN} fixed at $8a_0$ forming an angle θ_{HNN} with the r_{NH} axis fixed at = 5°; (◇) $NH(^3\Sigma^-)$; (□) $NH(^5\Sigma)$; (—), $NH(^3\Sigma^-)(R) + h(R)$; (— —), $NH(^3\Sigma^-)(R)$. The solid lines in the insets show $h(R)$, with all points referred to the $NH(^3\Sigma^-)$ diatomic. Key for panel **b**: (○) $N_2(^3\Pi_g)$; (◇) $N_2(^1\Sigma_g^+)$; (□) $N_2(^3\Sigma_u^+)$; (— - —) $N_2(^1\Sigma_g^+)(R)$; (— —) $N_2(^3\Pi_g)(R)$; (---) $N_2(^3\Sigma_u^+)(R)$. Filled symbols have been used to calibrate $k(x)$, with the solid lines showing $N_2(^3\Pi_g)(R)k(R) + N_2(^3\Sigma_u^+)(R)[1 - k(R)]$.

where r_i, θ_i and R_i are internal Jacobi coordinates (for the notation, see Figure 1 of ref 14), and $g_i = 1/2\{1 - \tanh[\xi(\eta R_i - R_j - R_k)]\}$ is a convenient damping function, with similar expressions for g_j and g_k. Following recent work on HCN[81] we have fixed $\eta = 6$ and $\xi = 1.0a_0^{-1}$. The damping function $\chi_n(r_i)$ was the same as for the diatomics, but using the center-of-mass separation for the relevant atom−diatom channel instead of R. The parameter ρ for both diagonal diabatic states was the one used for the single-sheeted potential energy surface of $HN_2(^2A')$,[2] were R_0 was taken as the average of the corresponding parameters for NO and SiH, which leads to $\rho = 15.9$.

For $n = 6$, 8, and 10, the atom−diatom dispersion coefficients are given by

$$C_n^{(i)}(R_i, \theta_i) = \sum_L C_n^L P_L(\cos\theta_i) \quad (46)$$

where $P_L(\cos\theta_i)$ denotes the L-th term of the Legendre polynomial expansion. For both diagonal diabatic states the $L = 0$, 2, and 4 components of this coefficients have been considered, with the internuclear dependences estimated as in ref 82, i.e., by using the generalized Slater−Kirkwood approximation[83] jointly with the dipolar polarizabilities, which have been calculated in the present work using the MRCI method with an AV*Q*Z basis set. The atom−diatom dispersion coefficients so calculated were then fitted to the form given in ref 83. For V_{11}, we have used the same dispersion coefficients as for the single-sheeted PES[2] of $HN_2(^2A')$. For V_{22}, the atom−diatom interactions must be understood under the constraints imposed by dissociation scheme discussed above, which would imply using two distinct atom−diatom dispersion coefficients for each channel. For simplicity, for the H−N_2 interaction, we have considered only the polarizabilities of $N_2(^3\Sigma_u^+)$, thence

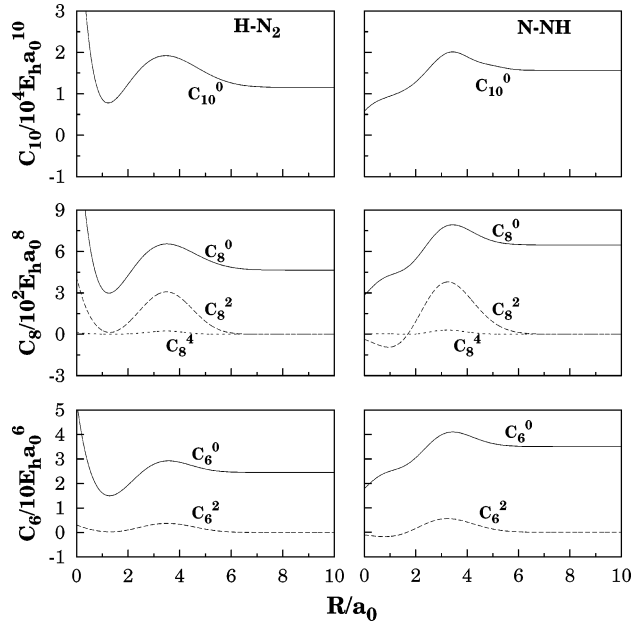

Figure 6. Atom−diatom dispersion coefficients for for the diabatic V_{22} state as a function of the corresponding internuclear distance.

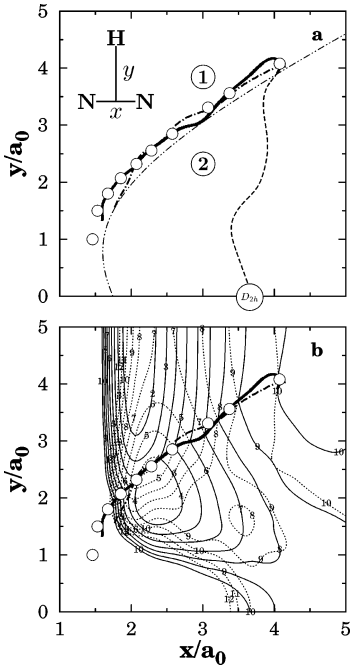

Figure 7. T-shaped crossing seam. Key for panel **a**: (○) calculated points; (− - −) as obtained from fitted diagonal states; (− −) as obtained from fitted adiabatic states without the damping function in eq 53; (—) as obtained from fitted adiabatic states with the above damping function. The dashed-dot (− ·· −) represents the $x_0(x)$ curve in eq 50. The numbers label the regions referred to in the text, while the large open circle indicates the D_{2h} conical intersection of the adiabatic states. Panel **b** shows also energy countours for the ground (—) and excited (---) states, in both cases starting at $E_0 = -0.3641E_h$ and equally spaced by $\Delta E_0 = 0.0385E_h$.

reducing the atom−diatom dispersion interaction on this channel to that for the $H(^2S) + N_2(^3\Sigma_u^+)$ interaction, which is truly applicable for $r_{N_2} \gtrsim 2.0a_0$. Similarly, for the N−NH channel, we have considered only the atom−diatom dispersion interaction referring to $N(^2D) + NH(^3\Sigma^-)$, which is an approximation for $r_{NH} \gtrsim 3.0a_0$. The resulting parameters are in Table 3 of the Supporting Information, with their internuclear dependences shown in Figure 6. As discussed elsewhere,[80] we have multiplied the two-body dynamical correlation energy for the *i*-th pair by $\prod_{l\neq i}[1 - g_l(\mathbf{R})]$, with corresponding factors for channels *j* and *k*, thus ensuring[80] that the only two-body contribution at the *i*-th channel is that of JK.

5.5. Three-Body Extended HF Energy and Fit of Diagonal Diabatic Terms. For these states, we start by removing, for a given triatomic geometry, the sum of the relevant two-body energy terms in eqs 30 and 32, modeled by EHFACE2U curves as described in section 5.3, and the three-body $[N(^2D) - N(^4S)]$-$F(\mathbf{R})$ term in eq 32 from the points obtained in section 4. This gives the total three-body energy for each of the diagonal diabatic states from where we now subtract the three-body dynamical correlation contribution modeled in section 5.4 to yield the three-body extended HF energy for each diagonal diabatic state referred to as $V^{(3)}_{11,EHF}(\mathbf{R})$ and $V^{(3)}_{22,EHF}(\mathbf{R})$ according to eq 31. To model the terms so obtained, we have employed the three-body distributed-polynomial form[84]

$$V^{(3)}_{n,EHF} = \sum_{j=1}^{N_n} P_n^{(j)}(Q_1, Q_2, Q_3) \sum_{i=1}^{3} \{1 - \tanh[\gamma^j_{n,i}(R_i - R^{j,ref}_{n,i})]\} \quad (47)$$

where the polynomials $P_n^{(j)}(Q_1, Q_2, Q_3)$ are written in terms of symmetry coordinates,[6] and the index *n* labels the diagonal diabatic state.

Regarding the linear fits, we follow basically the usual criterion but having in account the further complications arising from having stationary points at different geometries on the various diabatic terms. Specifically, we have chosen to center the polynomials at geometries close to the adiabatic stationary points, ensuring that each reference geometry was covered by diabatic points. The actual location has been finally decided by matters of convenience. The values of $\gamma^j_{n,i}$ were then obtained by trial-and-error, ensuring a representation of the crossing seams as accurately as possible. After obtaining a globally acceptable fit, we have centered lower-order polynomials at the van der Walls regions, and fine-tuned the calibration such as to obtain an accurate description of the long-range regions. The final total rmsd were lower than 1.4 kcal mol^{-1} for both diagonal diabatic states.

Figures 7 and 8 show the crossings seams predicted by the diagonal diabatic states, and Figures 3 and 4 illustrate the agreement between the diabatic points from section 4 and the fit. Panels **a**, **b**, and **c** of Figure 3 and insets therein show cuts of the diagonal diabatic terms from linear NNH to T-shaped configurations for r_{N_2} fixed at $1.854a_0$. As seen, the crossing is accurately mimicked, evolving smoothly to reproduce the adiabatic crossing seams as shown in Figures 7 and 8. The same behavior is exhibited for other r_{N_2} distances: $2.431a_0$ and $3.374a_0$. Panels **a**, **b**, and **c** of Figure 4 and insets therein illustrate the corresponding behavior for the other two channels with r_{NH} fixed at $2.465a_0$. Note the smooth evolution in going from a two conical intersection situation in NNH to no intersections for NHN linear arrangements. The remaining panels illustrate that the regions out of the range of both linear crossing seams is also accurately fitted, with the diabatic intersection disappearing as expected at linear geometries. Note that the C_{2v} region below the *ab initio* crossing seam in panel **a** of Figure 7 shows an evolution of the diabatic crossing with no support on the *ab initio* calculations, as discussed in the next section.

Figure 9 shows plots of the diagonal diabatic states for an atom moving around a partially relaxed diatomic. The notable feature is perhaps the fact that long range forces are smoothly

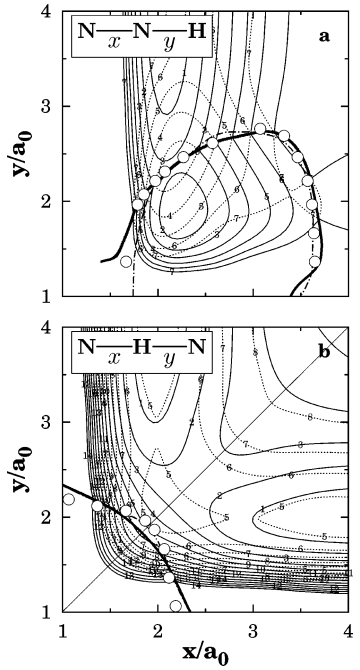

Figure 8. Linear crossing seams. Key for panels **a** and **b**: (○) calculated points; (− - −) as obtained from fitted diagonal states; (—) as obtained from fitted adiabatic states. Panel **a** shows energy countours for NNH arrangements in the ground (—) and excited (---) states, starting at $E_0 = -0.3641E_h$ and equally spaced by $\Delta E_0 = 0.04E_h$. Panel **b** shows contours for NHN arrangements with $E_0 = -0.1335E_h$ and $\Delta E_0 = 0.02E_h$.

(and accurately as far as the quality of the *ab initio* points allow) described in the diabatic sheets, ensuring a reliable description of the adiabatic long range behavior. The reference geometries $R_{n,i}^{j,\mathrm{ref}}$ and decay parameters $\gamma_{n,i}^{j}$ for the diabatic sheets are given in Tables 4 and 5 of the Supporting Information. These will be kept fixed when performing the final nonlinear least-squares of the adiabatic sheets.

5.6. The Nondiagonal Diabatic Linear Least-Squares Fit. To understand the T-shaped diagonal diabatic crossing behavior shown in Figure 7, we must explore the consequences of two properties introduced into the two sheets through the diabatization procedure. The first refers to having a common dissociation with the adiabatic states as shown in eqs 27, 30, and 32, and the second to the fact that the diagonal diabatic sheets interchange their role when passing through a seam.

The two numbers in Figure 7 label the two regions separated by the conical intersection. According to the diabatization procedure, we can state that close to **1** the diagonal states will follow the inequality $V_{22} > V_{11}$, while close to **2** it will be $V_{22} < V_{11}$. This inversion is responsible for the diagonal diabatic states being able to reproduce the crossing seam when modeled via single valued forms as in eqs 30 and 32.

If the molecule dissociates from region **2** via a path parallel to the *x*-axis, the three-body interaction will disappear and from eqs 30 and 32 one must have at a certain point onward

$$V_{11} \approx \mathrm{N_2}(^1\Sigma_g^+) + \mathrm{NH}(^3\Sigma^-) \tag{48}$$

and

$$V_{22} \approx \mathrm{N_2}(^3\Pi_g)k(x) + \mathrm{N_2}(^3\Sigma_u^+)[1 - k(x)] + \mathrm{NH}(^3\Sigma^-) + [N(^2D) - N(^4S)]F(\mathbf{R}) \tag{49}$$

Since $\mathrm{N_2}(^3\Pi_g)k(x) + \mathrm{N_2}(^3\Sigma_u^+)[1 - k(x)] + [\mathrm{N}(^2D) - \mathrm{N}(^4S)]F(\mathbf{R}) > \mathrm{N_2}(^1\Sigma_g^+)$, we must have $V_{22} > V_{11}$, which implies another inversion and hence another crossing. The same argument justifies why the crossing ends at the D_{2h} point signaled over the *x*-axis. In fact, we could say that the labels **1** and **2** define two distinct regions on the C_{2v} plane according to the crossing line, a dissociative region, characterized by relaxed configurations and where $V_{22} > V_{11}$, and an internal region, where $V_{22} < V_{11}$.

Yet, the *ab initio* calculations show that there is no support for the C_{2v} diabatic crossing, which must then be removed from the modeling. The solution requires that the condition $V_{12} = 0$ holds only for a specific region of the C_{2v} plane. Recall that we have fitted the T-shaped crossing points to a $y_T(x)$ function in eq 18. Since this gives the value of the coordinate $y_T(x)$ connecting the H atom to the center of N_2 along the C_{2v} crossing seam as a function of the NN bond distance *x*, we now require the form

$$x_0(y) = x_T(y) - d \tag{50}$$

with $d > 0$, where $x_T(y)$ corresponds to the NN bond distance as a function of *y* along the C_{2v} crossing seam. For this, $x_T(y)$ assumes the form

$$x_T(y) = c_0 + c_1 y + c_2 \exp[-\gamma(y + y_0)^2] \tag{51}$$

with the parameters given in Table 1 of the Supporting Information. In fact, the function $x_0(x)$ maps two regions of the C_{2v} plane, as shown in Figure 10, and we would prefer that the conical intersection were not present in the adiabatic states at region **2**. This would require involving a function f_T' that were identically zero at region **1** but nonzero at region **2**, such that $V_{12} = 0$ at region **1** and $V_{12} \neq 0$ at region **2**. A function that satisfies such criteria can be adapted from one utilized by one of us[10] during the construction of a multisheeted DMBE PES for $NO_2(^2A')$. We suggest using the analogous form

$$\begin{aligned} f_T'(x,y) &= 1 - \exp\{-\beta[1/z(x,y) - 1]^{n_T}\} && \text{if } z(x,y) < 1 \\ &= 0 && \text{if } z(x,y) \geq 1 \end{aligned} \tag{52}$$

where

$$z(x,y) = 1 + \tanh\{\alpha[x_0(y) - x]\}$$

with all parameters defined in Table 1 of the Supporting Information. Such a function is plotted in Figure 10. Note that the integer parameter n_T in eq 52 determines the order of the continuity. For our purposes, we have required continuity up to the second derivative, thus $n_T = 3$. The final $f_T(\mathbf{R})$ function in eq 33 will then be

$$f_T(\mathbf{R}) = f_T'(x,y) + Q(\mathbf{R})^2 \tag{53}$$

where $Q(\mathbf{R})$ is the angle-like variable[13]

$$Q(\mathbf{R}) = \frac{R_2 - R_3}{R_1} \tag{54}$$

responsible for removing the effects of $f_T(\mathbf{R})$ outside the C_{2v} plane. Note that regions **1** and **2** in Figure 10 [defined by $x_0(y)$ and used to create the function $f_T'(\mathbf{R})$] have a distinct definition from those labeled **1** and **2** in Figure 7 (defined according to the relative magnitude of the diagonal diabatic states in eqs 30

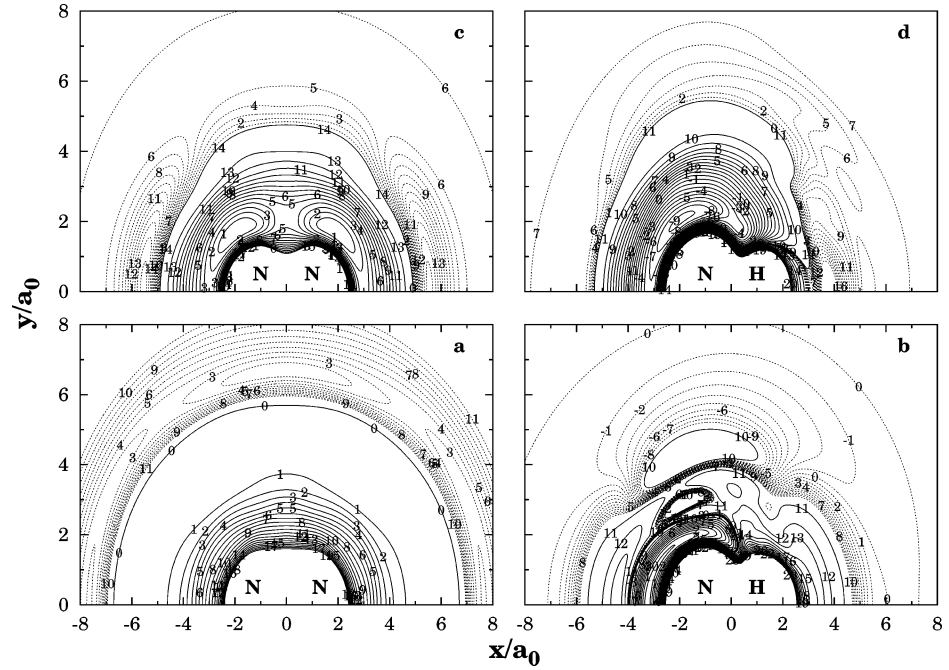

Figure 9. Panels **a** and **b** show the diabatic state V_{11} for the H−N_2 and N−NH channels, with panels **c** and **d** showing the same plots but for the diabatic V_{22} state. Initial isoenergy contours E_0 and spacings ΔE_0 in E_h are as follows (**a**) −0.3641 and 0.015 (solid); −0.3643 and 0.00001 (dotted); (**b**) −0.26 and 0.0125 (solid); −0.134 and 0.0004 (dotted); (**c**) −0.35 and 0.015 (solid); −0.13998 and 0.00075 (dotted); (**d**) −0.42 and 0.015 (solid); −0.045 and 0.0005 (dotted). The energy has been optimized withing the range $1.8 \le R_{N_2}/a_0 \le 2.4$ (panel **a**); $1.8 \le R_{NH}/a_0 \le 2.3$ (panels **b** and **d**); $2.2 \le R_{N_2}/a_0 \le 2.6$ (panel **c**).

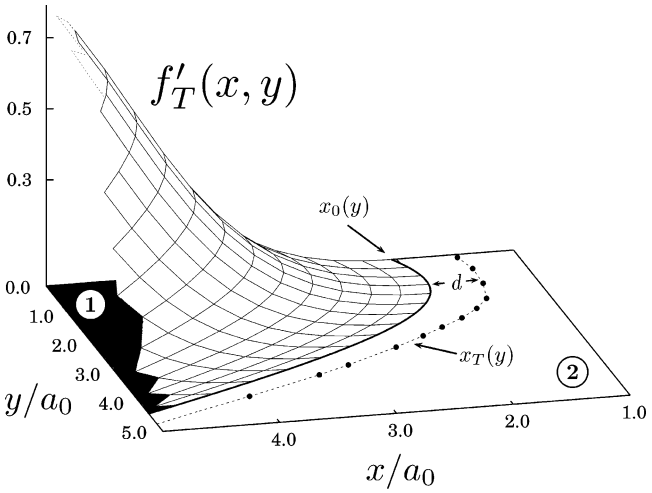

Figure 10. Damping function in eq 52. Also indicated is the region where it attains finite values (**1**) and vanishes identically (**2**). The dots show the calculated seam, fitted by $x_T(y)$ from eq 51 as shown by the dotted line, while the solid line shows the curve $x_0(y)$ from eq 50, which separates regions **1** and **2**.

and 32), but their parallel significance encouraged us to employ the same notation.

Finally, the $V^{(3)}_{12,EHF}(\mathbf{R})$ term in eq 33 is defined as

$$V^{(3)}_{12,EHF} = \sum_{j=1}^{N_{12}} P^{(j)}_{12}(Q_1, Q_2, Q_3) D^{(j)}_{12}(\mathbf{R}) \qquad (55)$$

with the dumping function $D^{(j)}_{12}$ given by

$$D^{(j)}_{12}(\mathbf{R}) = \prod_{i=1}^{3} \exp[\gamma^j_{12,i}(R_i - R^{j,ref}_{12,i})^2] \qquad (56)$$

with notation as in eq 47. A linear least-squares fit procedure was used to determine the linear coefficients, while the decay parameters $\gamma^j_{12,i}$ in eq 56 were determined by trial-and-error. The reference set $R^{j,ref}_{12,i}$ were chosen following the convenience of the fitting, with special attention to the boundary conditions imposed by f_T and f_l. Table 6 of the Supporting Information gathers the final values of $\gamma^j_{12,i}$ and $R^{j,ref}_{12,i}$.

TABLE 2: Stratified Root-Mean Squared Deviations (in kcal mol^{-1})

		maximum deviation		rmsd	
energy	no. of points	DMBE[a]	DMBE[b]	DMBE[a]	DMBE[b]
10	398	1.719	1.829	0.306	0.204
20	569	2.283	1.829	0.465	0.268
30	714	4.954	2.131	0.644	0.315
40	877	7.365	2.997	0.789	0.390
50	956	7.552	3.842	0.987	0.516
60	1058	7.806	3.842	1.058	0.559
70	1131	8.378	4.265	1.172	0.641
80	1188	8.378	5.432	1.242	0.694
90	1260	8.378	5.431	1.359	0.757
100	1451	8.378	5.688	1.463	0.800
125	1745	9.270	7.917	1.683	1.141
150	2519	9.662	10.671	1.737	1.326
175	3596	9.769	11.652	1.732	1.495
200	4561	9.953	13.696	1.822	1.631
300	5790	13.608	15.180	1.880	1.863
400	5895	13.608	15.180	1.921	1.971
500	5952	13.608	16.041	1.957	2.074
1000	6075	13.608	16.104	1.997	2.231
5000	6091	13.608	16.964	2.004	2.258

[a] This work, using preliminary estimate for coupled states; see text. [b] This work, final PES; see text.

6. Results and Discussion

The two adiabatic potentials $V^+(\mathbf{R})$ and $V^-(\mathbf{R})$ in eq 3 can now be formally obtained from the diabatic matrix in eqs 30, 32, and 33.

As emphasized in sections 4 and 5, the adiabatic states inherit from the diabatic ones the correct behavior at atom−diatom

TABLE 3: Other Stationary Points in the Lower Sheet of the 2 × 2 DMBE Potential Energy Surface

feature	property	DMBE[a]	DMBE[b]	DMBE[c]
T-shaped van der Waals	R_1/a_0	2.075	2.081	2.081
H···N_2	R_2/a_0	7.112	6.7773	6.857
	R_3/a_0	7.112	6.7773	6.857
	E/E_h	−0.3642	−0.364287	−0.3642
	$\Delta E^{d)}$	−0.07	−0.1175	−0.1
	ω_1(N−H)/cm^{-1}	69	93	105
	ω_2(N−N)/cm^{-1}	2337	2342	2343
	ω_3(bend)/cm^{-1}	18	8.5	21
linear van der Waals	R_1/a_0		2.081	2.081
H···N_2	R_2/a_0		6.6071	6.672
	R_3/a_0		8.6877	8.7527
	$\Delta E^{e)}$		1.1	1.5
	ω_1(N−H)/cm^{-1}		81	84
	ω_2(N−N)/cm^{-1}		2343	2343
	ω_3(bend)/cm^{-1}		7.7	10
saddle point linking	R_1/a_0		2.081	2.081
van der Waals minimums	R_2/a_0		6.5759	6.6084
H···N_2	R_3/a_0		7.9266	7.9096
	$\Delta E^{e)}$		4.0	6.6
	ω_1(N−H)/cm^{-1}		61	71
	ω_2(N−N)/cm^{-1}		2343	2343
	ω_3(bend)/cm^{-1}		18*i*	21*i*
linear TS	R_1/a_0	7.467	7.43	7.345
N−H···N	R_2/a_0	1.961	1.965	1.965
	R_3/a_0	5.506	5.465	5.380
	E/E_h	−0.1305	−0.1304	−0.1305
	$\Delta E^{f)}$	−0.2	−0.15	−0.2
	ω_1(N−H)/cm^{-1}	3198	4457	4444
	ω_2(N−N)/cm^{-1}	45	127	206
	ω_3(bend)/cm^{-1}	16	52*i*	278*i*
linear TS	R_1/a_0	6.846	6.818	6.558
N···N−H	R_2/a_0	1.965	1.964	1.964
	R_3/a_0	8.811	8.783	8.522
	E/E_h	−0.1304	−0.1305	−0.1307
	$\Delta E^{f)}$	−0.1	−0.16	−0.3
	ω_1(N−H)/cm^{-1}	4451	3260	4468
	ω_2(N−N)/cm^{-1}	119	34	182
	ω_3(bend)/cm^{-1}	56*i*	22*i*	80*i*
linear TS	R_1/a_0	4.758	4.740	4.6913
N···H···N	R_2/a_0	2.379	2.370	2.3457
	R_3/a_0	2.379	2.370	2.3457
	E/E_h	−0.0937	−0.0851	−0.0858
	$\Delta E^{f)}$	22.9	28.35	27.91
	ω_1(N−H)/cm^{-1}	2828*i*	3675*i*	3929*i*
	ω_2(N−N)/cm^{-1}	567	1368	2087
	ω_3(bend)/cm^{-1}	907	794*i*	333*i*

[a] Single-sheeted representation from ref 2. [b] This work, using preliminary estimate for coupled states; see the text. [c] This work, final PES; see the text. [d] Relative to H + N_2 asymptote (in kcal mol^{-1}). [e] Relative to the corresponding T-shaped van der Walls minimum (in cm^{-1}). [f] Relative to the N + NH asymptote (in kcal mol^{-1}).

dissociation while reproducing also the known crossing seams. However, the overall topography of the coupled states reveal some discrepancies relative to the *ab initio* points, mostly at the strong interaction region. To conform with the *ab initio* calculations, we have carried out a nonlinear least-squares fit for the linear coefficients of $V_{12}(\mathbf{R})$ in eq 55 using the values obtained from the linear fit in section 5.6 as a starting guess (the decay parameters $\gamma^j_{12,i}$ and reference sets $R^{j,\mathrm{ref}}_{12,i}$ have been held fixed at the values obtained from the linear fit). The diagonal diabatic states have been kept unaltered, as well as the damping functions f_l, f_T, and $D^{(j)}_{12}$ in eqs 33, 55, and 56. Thus, the atom−diatom dissociation limits remain identical as well as the locci of conical intersection.

The fifth column in Table 2 shows the stratified rmsd, taking the energy of the global minimun as reference. It is seen that up to 100 kcal mol^{-1}, where the lowest stationary points of the ground state are localized, such a DMBE PES would exhibit slightly larger rmsd than the single-sheeted DMBE PES of Poveda and Varandas.[2] However, as shown in Tables 1 and 3 (fourth column for results of the coupled states), a satisfactory description of the stationary point attributes within this energy range, including normal-mode frequencies, has already been achieved. For the long-range properties of the ground state such as van der Waals structures only minor discrepancies are observed, which is expected given the care taken in modeling such properties during the construction of the diagonal diabatic states. In fact, a qualitative satisfactory agreement between the Legendre components[85,86] of the ground state PES[2] and the present work is observed in Figure 13 up to reasonably high interaction regions.

A careful analysis has been performed regarding not only the adiabatic states themselves, but also the associated diabatic components. It has been found that many of the regions where significant deviations from the *ab initio* points existed correspond to relaxed molecular arrangements, were the polynomial form used for the non-diagonal diabatic state was strongly damped by the Gaussian terms in eq 56. This limited the fit at

TABLE 4: Important Structures of the Excited-State Potential Energy Surface

feature	property	DMBE[a]	DMBE[b]
minimum energy conical intersection for linear HNN arrangements	R_1/a_0	2.169	2.163
	R_2/a_0	2.366	2.369
	R_3/a_0	4.535	4.531
	E/E_h	−0.2729	−0.2728
	ΔE^c	53.7	53.7
minimum energy conical intersection for C_{2v} arrangements	R_1/a_0	2.253	2.236
	R_2/a_0	2.824	2.775
	R_3/a_0	2.824	2.775
	E/E_h	−0.2690	−0.2591
	ΔE^c	56.1	62.2
saddle point linking conical intersections	R_1/a_0	2.178	2.164
	R_2/a_0	3.922	3.763
	R_3/a_0	2.524	2.440
	E/E_h	−0.1855	−0.1905
	ΔE^c	108.5	105.4
	ω_1(N−H)/cm^{-1}	2863	3120
	ω_2(N−N)/cm^{-1}	1100	1879
	ω_3(bend)/cm^{-1}	1280i	1051i
C_{2v} local minimum	R_1/a_0	3.575	3.556
	R_2/a_0	2.395	2.397
	R_3/a_0	2.395	2.397
	E/E_h	−0.1087	−0.1033
	ΔE^c	156.8	160.2
	ω_1(N−H)/cm^{-1}	2356	4172
	ω_2(N−N)/cm^{-1}	3179	2871
	ω_3(bend)/cm^{-1}	1275	1449
barrier for H + N_2 linear insertion	R_1/a_0	2.452	2.427
	R_2/a_0	4.319	4.062
	R_3/a_0	6.771	6.489
	E/E_h	−0.1276	−0.1297
	ΔE^d	4.9	3.6
$D_{\infty h}$ local minimum	R_1/a_0	4.141	4.114
	R_2/a_0	2.071	2.057
	R_3/a_0	2.071	2.057
	E/E_h	−0.042	−0.042
	ΔE^e	−0.63	−0.63
	ω_1(N−H)/cm^{-1}	2893	2850
	ω_2(N−N)/cm^{-1}	755	845
	ω_3(bend)/cm^{-1}	371	371
barrier for N + HN linear insertion	R_1/a_0	4.765	4.895
	R_2/a_0	2.014	1.987
	R_3/a_0	2.751	2.908
	E/E_h	−0.0329	−0.0332
	ΔE^e	5.1	4.9

[a] This work, using preliminary estimate for coupled states; see text. [b] This work, final PES; see text. [c] Relative to the global minimum (in kcal mol^{-1}). [d] Relative to the H + N_2 asymptote (in kcal mol^{-1}). [e] Relative to the N + NH asymptote (in kcal mol^{-1}).

those regions and led us to speculate that it might have also inhibited any improvement of the fit at the remaining regions.

To improve the surfaces, we proceed with a more elaborated approach, consisting first of performing a nonlinear least-squares with all diabatic states. For this, we have attempted to improve the fit in relaxed molecular arrangements, mainly for the lower sheet, where the PES from ref 2 has been used as a reference for comparison. Special care has been taken to leave unaffected the crossing seams and atom−diatom dissociation channels, since the diagonal diabatic states were also involved in the fit. After analyzing the fit, some small discrepancies have been found to persist, mainly on the upper sheet. That may be explained by the intricate topography of this state[5] where at least two conical intersections are present.

The above discrepancies and other smaller ones have been removed by adding lower-order polynomials at the affected regions. Specifically, we have used the form

$$P_{(n)}(\mathbf{R}) = V^{(3)}_{\mathrm{EHF}}(\mathbf{R}) f_l(\mathbf{R}) Q(\mathbf{R})^2 \qquad (57)$$

where $V^{(3)}_{\mathrm{EHF}}$ is of the type of $V^{(3)}_{12,\mathrm{EHF}}$ in eq 55 but with lower order (2 and 3), $f_l(\mathbf{R})$ is the damping function in eq 34 and $Q(\mathbf{R})$ is the angle-like variable in eq 54. The index n numbers the polynomials. Note that $f_l(\mathbf{R})$ and $Q(\mathbf{R})$ ensure that the procedure leaves the crossing seams unaffected, while the Gaussian-damped forms in eq 58 were chosen to warrant that the discrepancies were handled as independently as possible. Tables 7 and 8 of the Supporting Information display the resulting parameters.

Shown in the last column of Table 2 is the resulting stratified rmsd for the final 2 × 2 DMBE PES. A significant improvement is observed up to 100 kcal mol^{-1} with respect to the previous fit, including the relevant stationary states; see Table 1 and panel **a** of Figure 11. Clearly, a smooth behavior has been achieved, with the major differences with respect to the single-sheeted DMBE PES[2] being the appearance of the conical intersections and the topography of the long range regions. Note that the occurrence of a double van der Waals minimum is inherent to the MRCI/AV*T*Z calculations as shown by the quality of the fit illustrated in the inset of panel **a** of Figure 12. Note further that this topology comes from the diabatic states and is insured via the fitted diabatization angle; see panel **a** of Figure 9 and eq 27. As also seen from the Legendre components of the potential in Figure 13, only minor changes have been introduced

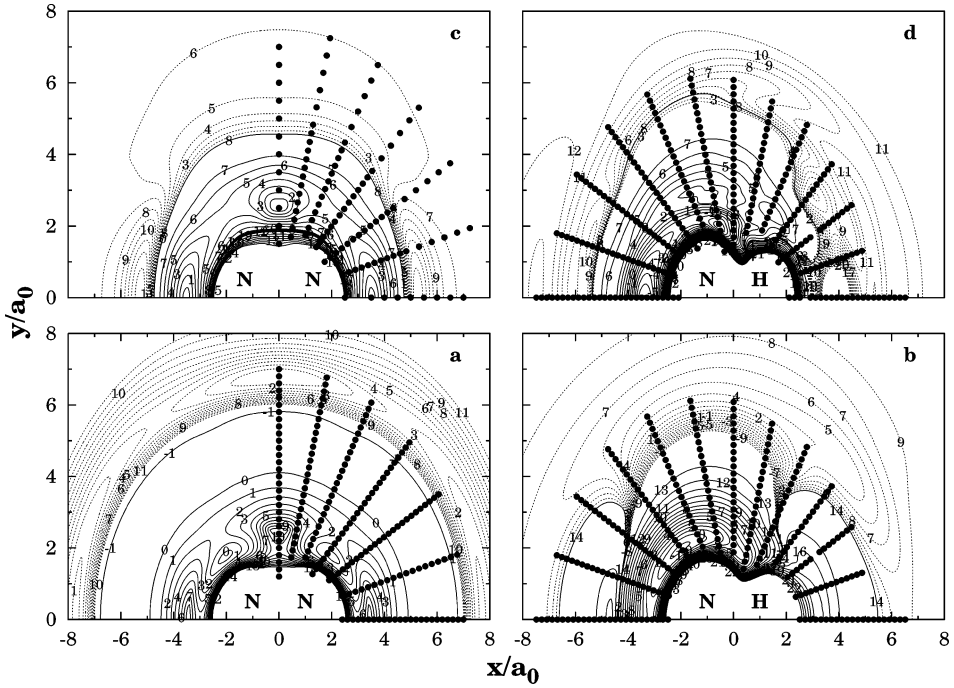

Figure 11. Panels **a** and **b** show the adiabatic state V^- for the H−N_2 and N−NH channels, while panels **c** and **d** show the corresponding plots for the adiabatic V^+ state. Initial isoenergy contours E_0 and spacings ΔE_0 in E_h are as follows: (**a**) −0.3641 and 0.008 (solid); −0.3643 and 0.00001 (dotted); (**b**) −0.355 and 0.015 (solid); −0.134 and 0.0002 (dotted); (**c**) −0.26 and 0.015 (solid); −0.13998 and 0.00075 (dotted); (**d**) −0.42 and 0.015 (solid); −0.045 and 0.0004 (dotted). The energy has been optimized as in Figure 9.

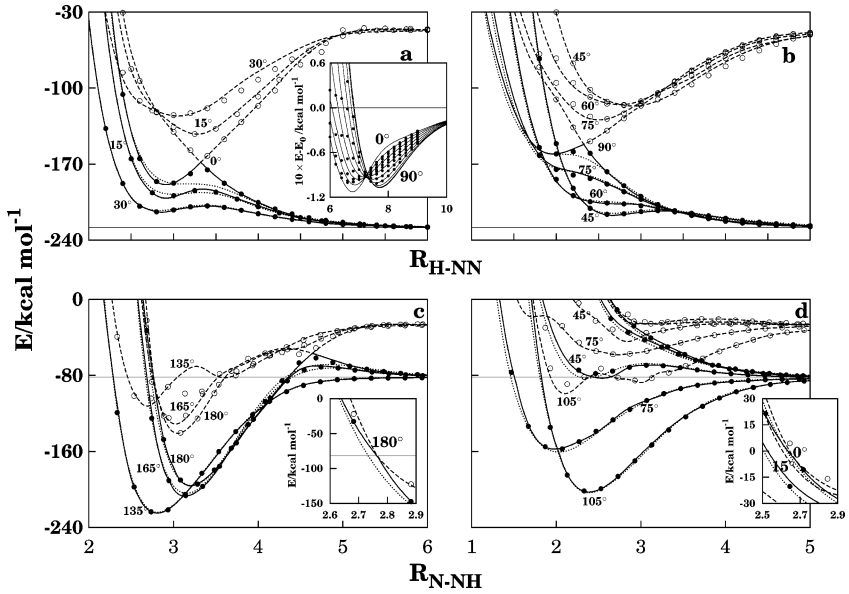

Figure 12. Adiabatic profiles and *ab initio* points for interactions with diatomics fixed at the ground state equilibrium geometry ($2.074a_0$ for r_{N_2}, and $1.965a_0$ for r_{NH}). Panels **a** and **b** refer to the H−NN channel and panels **c** and **d** to N−NH. Key for symbols: (● and —) $1^2A'$; (○ and − −) $2^2A'$; (---) PES for the $1^2A'$ state from ref 2. The points in the inset of panel **a** are referred to $E_0 = 228.8335$ kcal mol^{-1}.

with respect to the earlier fit. Interestingly, there is not much difference from the corresponding attributes of the single-sheeted PES,[2] despite the occurrence of a double-minimum van der Waals well. For the N−NH channel, the corresponding differences are also minor, except for the fact that the collinear saddle point in the present DMBE surface turns out to be a shallow minimum in ref 2.

The single-sheeted[2] and current 2 × 2 PESs are also compared in the profiles shown in Figures 3, 4, and 12. Except for the equilibrium diatomic geometry where the DMBE-SEC[42] method causes both surfaces to have the same energies at dissociation (see Figure 12), only small differences are exhibited due to differences in the one-electron basis sets and in the modeling. Keeping r_{N_2} fixed at $2.074a_0$ in the H−N_2 channel, we show in the first row of Figure 12 that the major discrepancies occur in the vicinity of the crossing seams which the single-sheeted PES cannot obviously reproduce. Note that in the neighborhood of the C_{2v} saddle point (shown in panels **a** and **b** of Figures 11 and 7; note that it is visible as "minima" in Figure 7) the differences are smaller as indicated by the corresponding attributes in Table 1. Similarly, for the N−NH channel, the differences between the single- and double-sheeted DMBE PESs is larger close to the conical intersections (see Figures 4 and 12 and insets therein). Figures 7 and 8 illustrate the shape of the crossing seams on the double-sheeted PES as predicted in

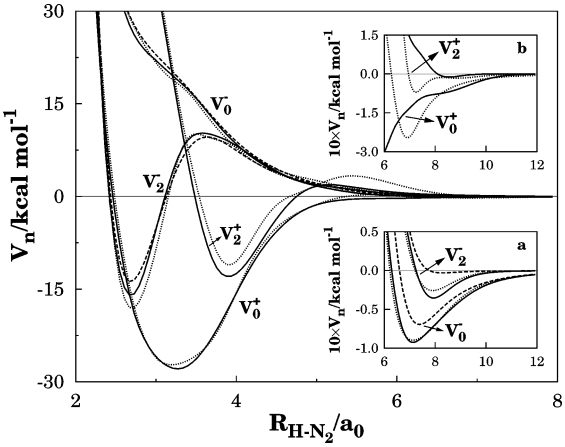

Figure 13. Legendre components of the upper V^- and lower V^+ adiabatic potentials. Key for curves: (—) final double-sheeted PESs; (---) preliminary adiabatic fit (see text); (— —), single valued PES from ref 2.

the earlier fit and the final one. Only small differences are observed, especially close to the N_2 equilibrium geometry ($2.074a_0$).

Regarding the excited state, we have three observations to make. First, the major discrepancies between the fit and the calculated *ab initio* energies arise as expected near the $2^2A'/3^2A'$ crossing seam (not modeled); see panels **d** and **g** (see inset therein) of Figure 3 and panel **a** of Figure 12. Such a crossing shows as an avoided crossing (maximum) in panel **c** of Figure 11. Second, the 2×2 DMBE PES shows the correct asymptotic behavior on dissociation by built construction via $F(\mathbf{R})$ in eq 39 and $k(x)$ in eq 44. Third, the attributes of the stationary points are all reasonably well reproduced in the fit; see Table 4. As for its long range part, the V_0 and V_2 Legendre components of the upper adiabatic PES for $H-N_2$ are shown in Figure 13. Despite the negative V_2 values (which implies that the insertion occurs preferentially with the atom—diatom vector aligned along the diatomic axis), we recall that a small collinear barrier (due to the maximum in panel **c** of Figure 11) may prevent the collinear attack of H to N_2. This suggests that higher Legendre components may still play a role.

As shown in Table 4, there are small local minima for C_{2v} and $D_{\infty h}$ arrangements. Since they lie at high energies above dissociation (see panels **b** of Figures 7 and 8), we only pay attention to the $D_{\infty h}$ that we have certified at the *ab initio* level. To correctly impose its location, we have added to the upper sheet the extra polynomial

$$P_{\mathrm{NHN}}(\mathbf{R}) = P_0 D_{12}(\mathbf{R}) f_l^2(\mathbf{R}) f_{\mathrm{T}}(\mathbf{R}) \tag{58}$$

where P_0 is an amplitude chosen to be 0.07015 E_h in order to correctly reproduce the same bending normal frequency as for the preliminary fit show in Table 3, D_{12} is a Gaussian-type damping function as in eq 56 with parameters values $\gamma_{12,1} = 10a_0^{-1}$, $\gamma_{12,2} = \gamma_{12,3} = 20a_0^{-1}$, $R_{12,1} = 4.114a_0$ and $R_{12,2} = R_{12,3} = 2.057a_0$ picked to localize the polynomial, with f_l and f_T used as above.

7. Concluding Remarks

We have reported an accurate global double-sheeted DMBE PES for the $1^2A'/2^2A'$ states of HN_2. All crossing seams were described to their full extent, with the ground state PES showing good agreement with the previously reported single-sheeted DMBE PES[2] except for regions close to the crossing seams where the present PES should obviously be preferred. For the excited state, a transition state connecting the T-shaped and NNH linear crossing seams as well as a linear barrier due to the avoiding $2^2A'/3^2A'$ crossing seams[5] are reported. For this state, two local minima, one for C_{2v} and the other for $D_{\infty h}$ arrangements have been also reported.

To face the intricate topology of HN_2, a novel diabatization scheme has been suggested. Although arbitrary to some extent as any other diabatization scheme,[87] we sustain that any diabatization scheme should be constructed such as to suit best a given application, with the proposed framework being found most useful when using polynomial-fitting techniques as employed in DMBE theory. The proposed scheme has the merit of warranting by built-in construction that the diabatic states will merge onto the adiabatic ones at the atom—diatom limits as schematized in eq 27. Such a warranty is not insured by direct diabatization schemes either providing diabatic wave functions[26,47—51] or diabatic energies.[62,63] The method can be classified as an indirect diabatization procedure that allows a well-defined global zeroth-order solution. In fact, it provides a diabatic grid of points with a proper description of the crossing seams in their full dimensionality, which is key for the study of nonadiabatic processes.[88] Indeed, it does not restrict neither the description of the involved crossing seams nor the accuracy of the model by using restricted, yet ingenious,[29,30,32—34,52] means for obtaining such zeroth-order solutions. Furthermore, it avoids introducing irregularities in the diabatic points except unavoidable ones inherent to the many-state *ab initio* calculations.[5,49] This contrasts with the dipole-moment strategy[9,38] where ambiguities arise both in defining the direction of dipole moment used for diabatization and by corrections that are subsequently required to obtain the diabatization angle. In fact, our experience suggests that corrections on the diabatization angle,[9,38,48,58] which are often necessary in many direct diabatization schemes,[48,58] must be avoided whenever possible at least when dealing with polynomial-fitting strategies. We emphasize that the method here suggested makes such corrections unnecessary by construction. Clearly, further applications using the current approach will be required to assess the method's usefulness. Work along these lines is currently in progress.

Acknowledgment. This work has the support of Fundação para a Ciência e a Tecnologia, Portugal (Contracts POCI/QUI/60501/2004, POCI/AMB/60261/2004, and REEQ/128/QUI/2005), under the auspices of POCI 2010 of Quadro Comunitário de Apoio III co-financed by FEDER.

Supporting Information Available: Tables showing the parameters in eqs 18—22, 24, and 50—52, parameters of the two-body extended Hartree—Fock energy, numerical values of the parameters in eq 46 for V_{22}, numerical values of the extended Hartree—Fock energy term in eqs 30, 32, and 33, and numerical values of parameters in eq 57 for the ground and excited states of HN_2. This material is available free of charge via the Internet at http://pubs.acs.org.

References and Notes

(1) Koizumi, H.; Schatz, G. C.; Walch, S. P. *J. Chem. Phys.* **1991**, *95*, 4130.

(2) Poveda, L. A.; Varandas, A. J. C. *J. Phys. Chem. A* **2003**, *107*, 7923.

(3) Caridade, P. J. S. B.; Poveda, L. A.; Rodrigues, S. P. J.; Varandas, A. J. C. *J. Phys. Chem. A* **2007**, *111*, 1172.

(4) Miller, J. A.; Branch, M. C.; Kee, R. J. *Combust. Flame* **1981**, *43*, 81.

(5) Mota, V. C.; Varandas, A. J. C. *J. Phys. Chem. A* **2007**, *111*, 10191.

(6) Murrell, J. N.; Carter, S.; Farantos, S. C.; Huxley, P.; Varandas, A. J. C. *Molecular Potential Energy Functions*; Wiley: Chichester, U.K., 1984.
(7) Varandas, A. J. C. In *Lecture Notes in Chemistry*; Laganá, A., Riganelli, A. Eds. Springer: Berlin, 2000; Vol. 75, p 33.
(8) Varandas, A. J. C. Vol. 15 of *Advanced Series in Physical Chemistry 15*; World Scientific Publishing: Singapore, 2004; Chapter 5, p 91.
(9) Boggio-Pasqua, M.; Voronin, A. I.; Halvick, P.; Rayez, J.-C.; Varandas, A. J. C. *Mol. Phys.* **2000**, *98*, 1925.
(10) Varandas, A. J. C. *J. Chem. Phys.* **2003**, *119*, 2596.
(11) Viegas, L. P.; Alijah, A.; Varandas, A. J. C. *J. Chem. Phys.* **2007**, *126*, 074309.
(12) Varandas, A. J. C. *J. Mol. Struct. THEOCHEM* **1985**, *120*, 401.
(13) Varandas, A. J. C. *Adv. Chem. Phys.* **1988**, *74*, 255−337.
(14) Varandas, A. J. C. *Chem. Phys. Lett.* **1992**, *194*, 333.
(15) Ballester, M.; Varandas, A. J. C. *Phys. Chem. Chem. Phys.* **2005**, *7*, 2305.
(16) Ellison, F. O. *J. Am. Chem. Soc.* **1963**, *85*, 3540.
(17) Tully, J. C. *Adv. Chem. Phys.* **1980**, *42*, 63.
(18) Kuntz, P. J. In *Atom-Molecule Collision Theory*; Bernstein, R., Ed.; Plenum: New York, 1979; p 79.
(19) Varandas, A. J. C.; Voronin, A. I. *Mol. Phys.* **1995**, *85*, 497.
(20) Varandas, A. J. C.; Voronin, A. I. *J. Phys. Chem.* **1995**, *99*, 15846.
(21) Preston, R. K.; Tully, J. C. *J. Chem. Phys.* **1971**, *54*, 4297.
(22) Kamisaka, H.; Bian, W.; Nobusada, K.; Nakamura, H. *J. Chem. Phys.* **2002**, *116*, 654.
(23) Domcke, W.; Woywod, C. *Chem. Phys. Lett.* **1993**, *216*, 362.
(24) Domcke, W.; Woywod, C.; Stengle, M. *Chem. Phys. Lett.* **1994**, *226*, 257.
(25) Atchity, G. J.; Ruedenberg, K. *Theor. Chem. Acc.* **1997**, *97*, 47.
(26) Nakamura, H.; Truhlar, D. G. *J. Chem. Phys.* **2001**, *115*, 10353.
(27) Pacher, T.; Cederbaum, L. S.; Köppel, H. *Adv. Chem. Phys.* **1993**, *84*, 293.
(28) Thiel, A.; Köppel, H. *J. Chem. Phys.* **1999**, *110*, 9371.
(29) Carter, S.; Murrell, J. N. *Mol. Phys.* **1980**, *41*, 567.
(30) Murrell, J. N.; Carter, S.; Mills, I. M.; Guest, M. F. *Mol. Phys.* **1981**, *42*, 605.
(31) Carter, S.; Mills, I. M.; Murrell, J. N.; Varandas, A. J. C. *Mol. Phys.* **1982**, *45*, 1053.
(32) Topaler, M. S.; Truhlar, D. G.; Chang, X. Y.; Piecuch, P.; Polanyi, J. C. *J. Chem. Phys.* **1998**, *108*, 5349.
(33) Hack, M. D.; Truhlar, D. G. *J. Chem. Phys.* **1999**, *110*, 4315.
(34) Jasper, A. W.; Hack, M. D.; Truhlar, D. G.; Piecuch, P. *J. Chem. Phys.* **2002**, *116*, 8353.
(35) Hay, P. G.; Pack, R. T.; Walker, R. B.; Heller, E. J. *J. Phys. Chem.* **1982**, *86*, 862.
(36) Macías, A.; Riera, A. *J. Phys. B: Atom. Molec. Phys.*. **1978**, *11*, 489.
(37) Werner, H.-J.; Meyer, W. *J. Chem. Phys.* **1981**, *74*, 5802.
(38) Dobbyn, A. J.; Knowles, P. J. *Mol. Phys.* **1997**, *91*, 1107.
(39) Werner, H.-J.; Knowles, P. J. *J. Chem. Phys.* **1988**, *89*, 5803.
(40) Dunning, T. H. *J. Chem. Phys.* **1989**, *90*, 1007.
(41) Kendall, R. A.; Dunning, T. H., Jr.; Harrison, R. J. *J. Chem. Phys.* **1992**, *96*, 6796.
(42) Varandas, A. J. C. *J. Chem. Phys.* **1989**, *90*, 4379.
(43) Lichten, W. *Phys. Rev.* **1967**, *164*, 131.
(44) Smith, F. T. *Phys. Rev.* **1969**, *179*, 111.
(45) O'Malley, T. *Adv. Atom. Mol. Phys.* **1971**, *7*, 223.
(46) Baer, M. *Mol. Phys.* **1980**, *40*, 1011.
(47) Woywod, C.; Stengle, M.; Domcke, W.; Flöthmann, H.; Schinke, R. *J. Chem. Phys.* **1997**, *107*, 7282.
(48) Heumann, B.; Weide, K.; Duren, R.; Schinke, R. *J. Chem. Phys.* **1993**, *98*, 5508.
(49) Simah, D.; Hartke, B.; Werner, H.-J. *J. Chem. Phys.* **1999**, *111*, 4523.
(50) Kurkal, V.; Fleurat-Lessard, P.; Schinke, R. *J. Chem. Phys.* **2003**, *119*, 1489.
(51) Grebenshchikov, S. Y.; Schinke, R.; Qu, Z.-W.; Zhu, H. *J. Chem. Phys.* **2006**, *124*, 204313.
(52) Brandão, J.; Rio, C. M. A. *J. Chem. Phys.* **2003**, *119*, 3148.
(53) Leforestier, C.; LeQuéré, F.; Yamashita, K.; Morokuma, K. *J. Chem. Phys.* **1994**, *101*, 3806.
(54) Qu, Z.-W.; Zhu, H.; Grebenshchikov, S. Y.; Schinke, R. *J. Chem. Phys.* **2005**, *123*, 074305.
(55) Dobbyn, A. J.; Connor, J. N. L.; Besley, N. A.; Knowles, P. J.; Schatz, G. C. *Phys. Chem. Chem. Phys.* **1999**, *1*, 957.
(56) Murrell, J. N.; Varandas, A. J. C. *Mol. Phys.* **1986**, *57*, 415.
(57) Kryachko, E. S.; Yarkony, D. R. *Int. J. Quantum Chem.* **2000**, *76*, 235.
(58) Flöthmann, H.; Beck, C.; Schinke, R.; Woywod, C.; Domcke, W. *J. Chem. Phys.* **1997**, *107*, 7296.
(59) Flöthmann, H.; Schinke, R.; Woywod, C.; Domcke, W. *J. Chem. Phys.* **1998**, *109*, 2680.
(60) Nakamura, H.; Truhlar, D. G. *J. Chem. Phys.* **2002**, *117*, 5576.
(61) Heumann, B.; Düren, R.; Schinke, R. *Chem. Phys. Lett.* **1991**, *180*, 583.
(62) Köppel, H.; Gronki, J.; Mahapatra, S. *J. Chem. Phys.* **2001**, *115*, 2377.
(63) Mahapatra, S.; Köppel, H.; Cederbaum, L. S.; Stampfuss, P.; Wenzel, W. *Chem. Phys.* **2000**, *259*, 211.
(64) Eyring, H.; Polanyi, M. *Z. Phys. Chem. B* **1931**, *12*, 279.
(65) Sato, S. *J. Chem. Phys.* **1955**, *23*, 2465.
(66) Kuntz, P. J.; Nemeth, E. M.; Polanyi, J. C.; Rosner, S. D.; Young, C. E. *J. Chem. Phys.* **1966**, *44*, 1168.
(67) Qu, Z.-W.; Zhu, H.; Grebenshchikov, S. Y.; Schinke, R.; Farantos, S. C. *J. Chem. Phys.* **2004**, *121*, 11731.
(68) Maierle, C. S.; Schatz, G. C.; Gordon, M. S.; McCabe, P.; Connor, J. N. L. *J. Chem. Soc., Faraday Trans.* **1997**, *93*, 709.
(69) Knowles, P. J.; Werner, H.-J. *Chem. Phys. Lett.* **1985**, *115*, 259.
(70) Brown, F. B.; Truhlar, D. G. *Chem. Phys. Lett.* **1985**, *117*, 307.
(71) Varandas, A. J. C.; Poveda, L. A. *Theor. Chem. Acc.* **2006**, *116*, 404.
(72) Murrell, J. N.; Carter, S. *J. Phys. Chem.* **1984**, *88*, 4887.
(73) Varandas, A. J. C.; Silva, J. D. *J. Chem. Soc. Faraday Trans.* **1992**, *88*, 941.
(74) Varandas, A. J. C. *Mol. Phys.* **1987**, *60*, 527.
(75) Le Roy, R. J. *Spec. Period. Rep. Chem. Soc. Mol. Spectrosc.* **1973**, *1*, 113.
(76) Varandas, A. J. C. *Phys. Sci.* (*Commun. At. Mol. Phys.*) **2007**, *76*, C28.
(77) Cooper, D. L.; Kirby, K. *J. Chem. Phys.* **1987**, *87*, 424.
(78) Jimeno, P.; Voronin, A. I.; Varandas, A. J. C. *J. Mol. Spectrosc.* **1998**, *192*, 86.
(79) Varandas, A. J. C.; Voronin, A. I. *Asian J. Spectrosc.* **1997**, *1*, 135.
(80) Varandas, A. J. C. *J. Chem. Phys.* **1996**, *105*, 3524.
(81) Varandas, A. J. C.; Rodrigues, S. P. J. *J. Phys. Chem. A* **2006**, *110*, 485.
(82) Varandas, A. J. C.; Rodrigues, S. P. J. *Chem. Phys. Lett.* **1995**, *245*, 66.
(83) Matías, M. A.; Varandas, A. J. C. *Mol. Phys.* **1990**, *70*, 623.
(84) Martínez-Núñez, E.; Varandas, A. J. C. *J. Phys. Chem. A* **2001**, *105*, 5923.
(85) Norbeck, J. M.; Certain, P. R.; Tang, K. T. *J. Chem. Phys.* **1975**, *63*, 590.
(86) Varandas, A. J. C. *J. Chem. Phys.* **1979**, *70*, 3786.
(87) Mead, C. A.; Truhlar, D. G. *J. Chem. Phys.* **1982**, *77*, 6090.
(88) Yarkony, D. R. *Mol. Phys.* **1998**, *93*, 971.